Rotational Transformation Methods for Radio Occultation and Passive Microwave Radiometry Colocation Analysis

by

Lucy Halperin

Submitted to the Department of Aeronautics and Astronautics
in partial fulfillment of the requirements for the degree of

Master of Science in Aeronautics and Astronautics

at the

MASSACHUSETTS INSTITUTE OF TECHNOLOGY

June 2021

Author .....
Department of Aeronautics and Astronautics
May 18, 2021

Certified by .....
Kerri Cahoy
Associate Professor
Thesis Supervisor

Accepted by .....
Zoltan Spakovszky
Professor, Aeronautics and Astronautics
Chair, Graduate Program Committee

Rotational Transformation Methods for Radio Occultation and Passive Microwave Radiometry Colocation Analysis

by

Lucy Halperin

Submitted to the Department of Aeronautics and Astronautics
on May 18, 2021, in partial fulfillment of the
requirements for the degree of
Master of Science in Aeronautics and Astronautics

Abstract

Global Navigation Satellite System Radio Occultation (GNSS-RO) and passive microwave radiometry (MWR) provide useful atmospheric profiles for inputs into Numerical Weather Prediction models. However, both remote sensing techniques face unique challenges that require auxiliary atmospheric data to mitigate. GNSS-RO provides extremely high vertical resolution retrievals in the Marine Boundary Layer but by itself is unable to distinguish between the contributions of water vapor and the "dry" atmosphere. MWR instruments have inherent biases in antenna temperature. GNSS-RO and MWR measurements taken within the same atmospheric volume at approximately the same time are mutually beneficial: each sensing technique provides the constraints needed by the other to solve its aforementioned profiling issue. This work introduces a fast, approximate method for analyzing the presence of colocated GNSS-RO/MWR measurements that requires only Two-Line Element (TLE) MWR data. The method applies a rotational transformation to map GNSS-RO soundings into the coordinate system natural to a cross-track scanning MWR satellite. The rotational transformation method is compared to the typical "brute force" colocation determination method and found to compute colocations 20x faster, with an average accuracy within 1.5% of "brute force" colocated occultations. Two initial applications of the rotational transformation colocation determination method are explored: a comprehensive study of the colocations occurring among active GNSS-RO and MWR missions, and colocation analysis of a proposed MWR constellation aimed to maximize colocations with the COSMIC-2 constellation.

Thesis Supervisor: Kerri Cahoy
Title: Associate Professor

Acknowledgments

This thesis was made possible by the technical and emotional support of many fellow researchers, friends, and family members. Without you all, I would not be where I am today.

First and foremost, I would like to express my gratitude to my graduate advisor, Professor Kerri Cahoy. Thank you so much for all the technical knowledge and leadership you have provided over the past two years. It has been an honor to work with you and be a part of STARLab. I would like to extend my thanks to all members of the AER/MIT research group: Dr. Stephen Leroy and Dr. Riley Fitzgerald for your continued patience and willingness to answer my many radio occultation-related questions, Alex for your coding skills that put mine to shame, and Amelia for your friendship, positivity, and humor - your camaraderie made writing a master's thesis during a global pandemic bearable.

My friends have ridden the highs of the past two years with me and shown me more than enough love to help me through the lows. To the members of the Kusters Kluster - Faisal, Katie, and Ryan - you all have been the highlight of my time in graduate school and the best labmates I could ask for. Thank you for welcoming me into STARLab, answering my many thesis questions, and spontaneously Facetiming me at all hours to keep me sane. Long live the snack drawer. To my roommates: many thanks to Andrew for the hours spent editing my thesis and teaching astrodynamics to me and to Bailey for providing a secondary work-from-home office and countless support Oreos. To Megan, my best friend and one of my biggest cheerleaders, thank you for always being on the other end of the phone.

And finally, an enormous thank you to my family, who have always been an invaluable source of support. Thank you to my parents, grandparents, brother Taylor, and cousin Sam for your unwavering belief in me, your role modeling of what it means to be passionate about learning, and your encouragement to always be curious about the world around me. This thesis is dedicated to my Zaidy, who embodied what it means to be an engineer. I love you guys.

THIS PAGE INTENTIONALLY LEFT BLANK

Contents

THIS PAGE INTENTIONALLY LEFT BLANK

List of Figures

THIS PAGE INTENTIONALLY LEFT BLANK

List of Tables

THIS PAGE INTENTIONALLY LEFT BLANK

List of Acronyms

AMSR-E	Advanced Microwave Scanning Radiometer for Earth Observing System
AMSU	Advanced Microwave Sounding Unit
ATMS	Advanced Technology Microwave Sounder
BFCD	Brute Force Colocation Determination
BS	Background Simulation
CDAAC	COSMIC Data Analysis and Archive Center
CLASS	Comprehensive Large Array-data Stewardship System
CORISS	C/NOFS Occultation Receiver for Ionospheric Sensing and Specification
COSMIC	Constellation Observing System for Meteorology, Ionosphere, and Climate
CRTM	Community Radiative Transfer Model
ECEF	Earth-Centered Earth-Fixed
ECI	Earth-Centered Inertial
EC-RO	Earth-Centered Radio Occultation
ESA	European Space Agency
EUMETSAT	European Organisation for the Exploitation of Meteorological Satellites
FY-3C	Fengyun-3C
FY-3D	Fengyun-3D
GNOS	Global Navigation Satellite System Occultation Sounder
GNSS	Global Navigation Satellite System
GOLPE	GPS Occultation and Passive reflection Experiment

GPS	Global Positioning System
GRAS	Global Navigation Satellite Systems Radio Occultation Receiver for Atmospheric Sounding
HSB	Humidity Sounder for Brazil
IGOR	Integrated GPS and Occultation Receiver
LEO	low Earth orbit
MBL	Marine Boundary Layer
MEO	medium Earth orbit
MetOp	Meteorological Operational
MHS	Microwave Humidity Sounder
MWHS	Microwave Humidity Sounder
MWR	Microwave Radiometer
MWS	Micro-Wave Sounder
MWTS	Microwave Temperature Sounder
NOAA	National Oceanic and Atmospheric Administration
NORAD	North American Aerospace Defense Command
NWP	Numerical Weather Prediction
OSCAR	Observing Systems Capability Analysis and Review
PBL	Planetary Boundary Layer
RAAN	Right Ascension of the Ascending Node
RO	Radio Occultation
ROSA	Radio Occultation Sounder of the Atmosphere
RTCD-G	Rotational Transformation Colocation Determination Generalized
RTCD-SS	Rotational Transformation Colocation Determination Sun-Synchronous
RTM	Radiative Transfer Model
SAPHIR	Sondeur Atmospherique du Profil d'Humidite Intertropicale par Radiometrie
SNO	Simultaneous Nadir Overpass

TanDEM-X	TerraSAR-X Add-oN for Digital Elevation Measurement
TEME	True Equator Mean Equinox
TGRS	Tri GNSS Radio-occultation System
TLE	Two-Line Element
TMS	TROPICS Millimeter-wave Sounder
TROPICS	Time-Resolved Observations of Precipitation structure and storm Intensity with a Constellation of Smallsats
UCAR	University Corporation for Atmospheric Research
WMO	World Meteorological Organization

THIS PAGE INTENTIONALLY LEFT BLANK

Chapter 1

Introduction

Accurate weather forecasting and climate modeling are beneficial to the well-being of humanity. Numerical Weather Prediction (NWP), the method through which weather forecasting is performed, can save lives, mitigate impact and financial loss from extreme weather, and help various sectors (such as energy, agriculture, transportation, and recreation) generate substantial financial revenue. NWP has improved significantly over the past 40 years [12]. With each passing decade, forecast skill increases by one day (i.e., a four day forecast this year is as accurate as a three day forecast ten years ago) [12]. However, a number of challenges still plague our ability to make further strides in weather prediction [12]. Insufficient observational data in certain regions, limited computational power, and biased weather measurements limit NWP forecasting accuracy.

Global Navigation Satellite System (GNSS) Radio Occultation (RO) instruments on satellites and cross-track scanning microwave radiometry (MWR) sounding instruments on satellites provide two crucial sources of observational inputs to NWP models [14, 17]. Each observational source has unique issues with biased measurements that, if corrected, have the potential to improve NWP weather prediction and climate modeling [14, 22]. Observations from separate instruments are "colocated" when the observations occur within a specific distance and time window from one another. Colocations between GNSS-RO and MWR missions provide a solution to GNSS-RO and MWR instrument bias. This thesis presents a new method for locating

GNSS-RO/MWR colocations that requires only MWR Two-Line Element (TLE) data and comprehensive GNSS-RO data, assesses how well the method performs, applies the method to survey where colocations presently occur among active missions, and uses the method to assess where colocations may occur among theoretical missions.

1.1 Benefits of GNSS-RO/MWR Colocations: Marine Boundary Layer Profiling

The region of the Planetary Boundary Layer (PBL) over the ocean, known as the Marine Boundary Layer (MBL), is crucial to climate and weather modeling. Unfortunately, the remote nature of much of the MBL makes the use of traditional sensing techniques such as tower measurements and field observations difficult. Since the height of the MBL is only about 2 kilometers and is often cloud-covered, remote sensing instruments such as radiosondes and microwave radiometers have difficulty characterizing MBL structure [36]. GNSS-RO is uniquely able to profile the MBL due to its global coverage, high vertical resolution, and ability to penetrate through clouds [9].

The top of the MBL has sharp moisture gradients and strong temperature inversion which often causes a phenomenon called "super-refraction" or "ducting." Super-refraction can cause extreme negative bias in GNSS-RO refractivity profiles, known as N-bias (where N is refractivity) [33]. Super-refraction occurs when the vertical refractivity gradient in the MBL becomes so large that the radius of curvature of the bent GNSS signal becomes less than the radius of the Earth ($\mathrm{d}N/\mathrm{dz} < 157$ N-units km^{-1}, where z is the height of the atmospheric layer above the Earth's surface). Due to the geometry of GNSS radio occultations, no ray tangent point exists within the ducting layer for an external ray that begins and ends outside of the atmosphere. As a result, the Abel transform which is used to relate GNSS-RO bending angles to refractivity profiles cannot find a unique solution and instead outputs the lowest refractivity solution of all the possible solutions [41]. The N-bias in GNSS-RO re-

fractivity measurements caused by super-refraction can be up to -15% at the top of the MBL and -4% at Earth's surface [33, 40].

In order to effectively use GNSS-RO to profile the MBL, the negative bias caused by super-refraction must be mitigated. Xie et al. (2006) present a method to eliminate bias and reconstruct refractivity profiles within the MBL [41]. A nonlinear function is used to relate the Abel-retrieved refractivity profile to the continuum of possible profiles associated with the given bending angle. The closest profile to the "truth" can be selected using a number of constraints, including the impact parameter and the upper limit of the ducting layer. This reconstruction method has been successfully used in simulation, but obtaining accurate values for the required constraints is difficult in operational retrievals [40].

Cross-track scanning microwave radiometers can provide auxiliary data needed to assist super-refraction parameterization to characterize MBL structure. Colocated MWR profiles serve as an external constraint to the reconstruction method introduced by Xie et al. (2006). Precipitable water retrievals from the Advanced Microwave Scanning Radiometer for Earth Observing System (AMSR-E) have already been used in conjunction with a modified reconstruction method to reduce N-bias to less than -1% in simulation and less than -5% in actual cases [36]. Precipitable water vapor, though, is just a single constraint on GNSS-RO retrieval in super-refraction conditions, equivalent to one MWR channel that is sensitive to water vapor, but weakly so. If several MWR radiance channels are considered instead, especially with sensitivity to both temperature and water vapor, MWR data can constrain GNSS-RO retrievals in the MBL more strongly. Assessing the existing GNSS-RO/MWR colocations and having the ability to design constellations to maximize these colocations would be beneficial to the future of MBL profiling and weather forecasting.

1.2 Benefits of GNSS-RO/MWR Colocations: Correction of MWR Bias

Cross-track scanning MWR instruments have inherent calibration-related biases and bias trends in antenna temperature that need to be corrected in order to provide consistent, accurate measurements for weather monitoring. These biases result from a number of different sources:

- Scan angle bias due to radiation reflected off of the satellite hosting the MWR instrument [23]
- Drifts and uncertainties in channel center frequencies [30]
- Cold calibration error sources (uncertainty in cosmic background temperature) [34]
- Hot calibration error sources (uncertainty in blackbody physical temperature and emissivity) [34]
- Calibration transfer function error sources (error in modeling the relationship between voltages detected by radiometer and brightness temperature due to uncertainty in nonlinearities, system noise, system gain drift, and bandpass shape changes) [42, 34]
- Instrument degradation over time and other satellite specific biases [42]

Validation of MWR data using measurements from other weather monitoring satellites can help mitigate such biases. Two methods of validation are primarily used: Simultaneous Nadir Overpass (SNO) and Radiative Transfer Model (RTM) Background Simulation (BS) [22].

The SNO method leverages colocations between soundings from different MWR satellites by taking advantage of the fact that many polar orbiting MWR satellites have slightly different periods and occasionally view the same nadir location at the

same time (within ∼30 seconds of one another) [22]. When such a colocation occurs, calibration differences for spectrally matched channels on the two spacecraft can be identified. SNO's requirement of a close time match up between the colocated measurements limits the number of qualifying colocations.

The RTM-BS method leverages colocations between MWR soundings and GNSS-RO soundings. Pressure, temperature, and water vapor profiles from GNSS-RO data are used to establish boundary conditions for an RTM which is then used to simulate brightness temperatures. The simulated brightness temperature values are compared to the colocated radiance values observed by the MWR instrument. Subtracting the simulated values (B) from the observed values (O) give O-B antenna temperature biases that quantify MWR error. GNSS-RO data have unique strengths in helping to correct MWR calibration error. GNSS-RO receivers continuously "self-calibrate" using GNSS signals that are not attenuated by the atmosphere [23]. These GNSS signals are monitored and corrected by atomic clocks, causing the signal timing to be known with high accuracy [10]. This leads to high accuracy of GNSS-RO data and high consistency between measurements from different GNSS-RO satellites [18]. The RTM-BS method has less stringent colocation time match up requirements than SNO; measurements must be within several hours of one another, rather than within a minute.

Mitigation of MWR calibration bias through the use of GNSS-RO profiles has extensive heritage. The Global Navigation Satellite System Occultation Sounder (GNOS) data onboard the Chinese Fengyun-3C satellite was used to calibrate the Microwave Temperature Sounder (MWTS) instrument and Microwave Humidity Sounder (MWHS) instrument onboard the Fengyun-3D satellite [21]. Colocated RO data under clear skies and over oceans were used as inputs into a Community Radiative Transfer Model (CRTM) to quantify biases of MWTS and MWHS observations. Global Navigational Satellite System Receiver for Atmospheric Sounding (GRAS) data from the MetOp-A and MetOp-B satellites were used to quantify intersatellite biases between the Advanced Microwave Sounding Unit-A (AMSU-A) onboard the NOAA-15, NOAA-16, NOAA-18, and MetOp-A satellites [23]. Colocated GRAS measurements

were used with an RTM to find disparities between the different AMSU-A sensors and to determine how instrument bias varies with instrument scan angle. GNSS-RO data from the COSMIC-1 constellation were used to calibrate AMSU-A data from NOAA-18, NOAA-19, MetOp-A, and MetOp-B and Advanced Technology Microwave Sounder (ATMS) data from Suomi-NPP and NOAA-20 [22]. Colocated RO data are used with a CRTM to quantify AMSU-A and ATMS bias [22].

1.3 Benefits of Fast, Approximate Method for Colocation Prediction

Determining where and when colocated measurements occur is presently a computationally expensive undertaking. Comprehensive datasets of RO soundings for the GNSS-RO satellite of interest and comprehensive datasets of MWR soundings for the MWR satellite of interest are needed. For every occultation, every MWR sounding must be iterated through to determine if the given occultation has a MWR sounding that fits within the colocation criteria. Calculating one day's worth of colocations between one GNSS-RO mission and one MWR mission can take as long as $\sim$15 minutes. While several papers show where colocated GNSS-RO/MWR observations occur among a few specific missions, none 1) perform a comprehensive study to determine where and how many existing colocations there are among all active missions or 2) predict where colocations will occur among future GNSS-RO and MWR missions [22, 23, 21, 29].

The advent of a fast, approximate method for colocation prediction that requires only Two-Line Element (TLE) MWR data enables quick colocation determination that runs on the order of 20x faster than the typical, computationally expensive method. The absence of requirement of a full MWR dataset makes colocation determination for future missions easier: it is far less challenging to simulate TLE files than entire MWR datasets. Colocation density can be quickly estimated and thus potentially included as a factor in GNSS-RO and MWR mission design.

1.4 Thesis Structure

Chapter 1 describes the rationale behind the development of a fast, approximate method for predicting GNSS-RO/MWR colocations.

Chapter 2 explains the fundamental concepts behind GNSS-RO and MWR remote sensing. A summary of past, present, and future GNSS-RO and MWR missions is given. The missions considered for colocation analysis in this thesis are identified.

Chapter 3 presents the approach in this work, using three methods for GNSS-RO/MWR colocation determination: the typical method used in past colocation analyses and two variations of a novel, fast, approximate method. The mathematical formulas used to determine if GNSS-RO and MWR measurements are spatially and temporally colocated are given for each method.

Chapter 4 gives a performance assessment of the two novel methods for colocation determination. The theory outlined in Chapter 3 is validated and the novel methods are compared to the typical method used in past colocation analyses to quantify the error of the novel methods.

Chapter 5 provides two example applications of the novel methods for colocation determination. Colocations occurring already among 12 active GNSS-RO satellites and 7 active MWR satellites are estimated. Colocations from a theoretical MWR constellation designed to trail the COSMIC-2 constellation are assessed.

Chapter 6 summarizes the findings of this thesis and offers next steps for improving and applying the new colocation determination methods.

THIS PAGE INTENTIONALLY LEFT BLANK

Chapter 2

Background

This chapter provides background on the two remote sensing techniques considered in this thesis: Global Navigation Satellite Systems Radio Occultation (GNSS-RO) and Microwave Radiometry (MWR) using cross-track scanning microwave sounders. A description of each remote sensing technique is provided, as well as a summary of the retired, active, and planned missions performing these sensing techniques. The missions considered during colocation analysis in Chapters 4 and 5 are identified.

2.1 GNSS Radio Occultation

2.1.1 GNSS Radio Occultation Geometry

GNSS-RO is an active limb-sounding technique used to produce refractivity profiles of the Earth's atmosphere. A GNSS-RO event occurs when a radio signal is sent from a global navigation satellite in medium Earth orbit (MEO), travels through the atmosphere, and is received by a satellite in low Earth orbit (LEO). The correct geometry to enable a GNSS-RO event happens when the global navigation satellite is occulted by the Earth and thus appears to rise or set from the perspective of the LEO satellite. As the emitted radio signals travel through the atmosphere, they are bent and delayed as a result of atmospheric refractive index gradients [31]. Figure 2-1 depicts the geometry of a radio occultation event. For neutral atmosphere GNSS-RO,

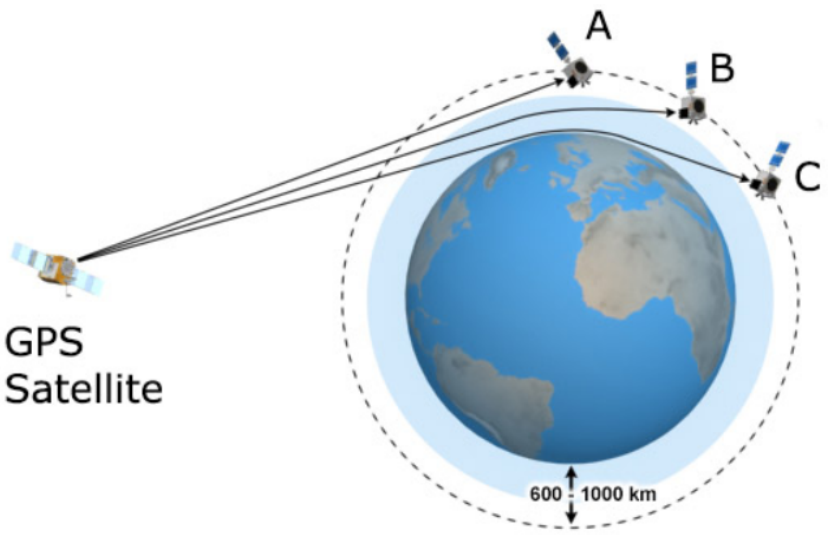

Figure 2-1: The geometry is shown for a setting GNSS-RO event. When the receiving satellite is in Position A, the radio signal sent from the navigation satellite does not pass through the atmosphere and therefore travels in a straight line. When the receiving satellite is in Position B, the radio signal must pass through the upper layer of the atmosphere and thus is slightly bent. To arrive at Position C, the radio signal passes through the upper and lower atmosphere and consequently is bent more [5].

a rising occultation event begins when the radio signal path grazes the Earth's limb and ends when it passes through the mesopause. A setting occultation event follows a reverse trajectory (shown in Figure 2-1). An occultation event typically lasts 1-2 minutes [31].

2.1.2 GNSS Radio Occultation Atmospheric Science

GNSS receivers onboard the satellite in LEO measure the phase and amplitude of the received radio signal. The bending shown in Figure 2-1 causes a phase delay in the signal. By measuring the phase shift in the radio signal over the course of the occultation event and differentiating this shift with respect to time, signal frequency shifts are calculated. Frequency shifts are used to calculate profiles of bending angles, which in turn can be used to calculate profiles of atmospheric refractivity [31]. In the stratosphere and upper troposphere, these atmospheric refractivity profiles provide information on temperature and pressure. Below the tropopause, the presence of water vapor limits the accuracy of temperature and pressure profiles, but allows for

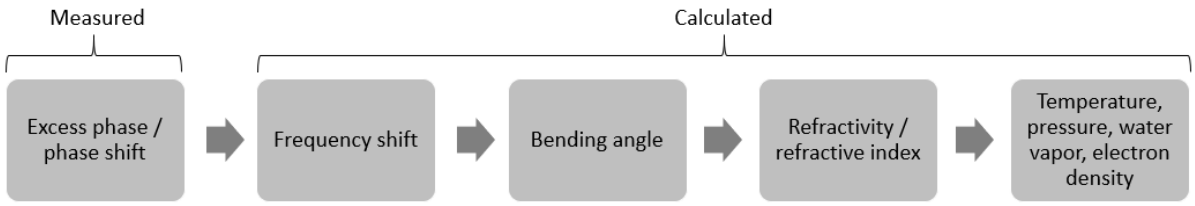

Figure 2-2: GNSS-RO measurements require several processing steps to obtain the desired atmospheric data.

the recovery of water vapor profiles given temperature data from other sources [9]. In the ionosphere, information on vertical electron density can be extracted [24]. A summary of the process used to produce useful atmospheric profiles from received radio signals is shown in Figure 2-2.

GNSS-RO produces measurements with extremely high vertical resolution: 0.1 kilometers near Earth's surface, 0.2 kilometers in the troposphere, and 1.5 kilometers in the stratosphere [11]. GNSS-RO observations have both high accuracy ($<$ 1K for temperature profiles) and high precision (0.02 - 0.05K for temperature profiles) [9]. GPS satellites transmit on L1 (1575.42 MHz) and L2 (1227.60 MHz) frequencies, meaning that signal wavelengths are long enough to be only minimally affected by precipitation, clouds, and aerosols, and thus can provide global coverage [11]. GNSS-RO is "self-calibrated" (requiring no external calibration), has no instrument drift, and has no satellite-to-satellite bias [9]. The combination of the aforementioned properties make GNSS-RO an excellent candidate to act as a calibration source for other remote sensing systems.

2.1.3 Selected Radio Occultation Missions

A list of space-based public sector GNSS-RO missions is provided in Table 2.1. Missions that are highlighted in the table are used for colocation analysis in this thesis.

The performance assessment of colocation determination methods (Chapter 4) uses data from the Constellation Observing System for Meteorology, Ionosphere, and Climate-2 (COSMIC-2) constellation and the Meteorological Operational (MetOp) constellation. The COSMIC-2 and MetOp constellations are both active GNSS-RO

missions. COSMIC-2 is used for performance assessment of colocation determination methods since it experiences more occultations per day than any other existing GNSS-RO mission. MetOp is selected since it hosts both a GNSS receiver and a cross-track MWR sounder.

Analysis of existing colocations happening among active GNSS-RO and MWR missions (Chapter 5) considers the COSMIC-2 and MetOp constellations, and additionally includes the TerraSAR-X, TanDEM-X, and ROHP-PAZ satellites. The remaining active GNSS-RO missions listed in Table 2.1 are excluded due to data inaccessibility.

A brief description of each of the GNSS-RO missions used for colocation analysis is included here:

COSMIC-2: COSMIC-2 is a joint US-Taiwan, six satellite constellation launched in June 2019. The constellation is in a 24° inclination orbit at an altitude of 520[1] kilometers [4] . COSMIC-2 utilizes the Tri GNSS Radio-occultation System (TGRS), allowing each satellite to receive signals from the GPS and GLONASS global navigation constellations. The constellation provides approximately 4000-5000 radio occultation soundings per day [15].

MetOp-A/B/C: The MetOp constellation is comprised of three satellites (MetOp-A, MetOp-B, and MetOp-C) launched in 2006, 2012, and 2018 respectively. The constellation was developed by the European Space Agency (ESA) and is operated by the European Organisation for the Exploitation of Meteorological Satellites (EUMETSAT). Each satellite is in a 98.7° inclination sun-synchronous orbit at an altitude of 817 kilometers. The MetOp constellation utilizes the Global Navigation Satellite System Receiver for Atmospheric Sounding (GRAS), allowing each satellite to receive signals from the GPS global navigation constellation. Each satellite in the constellation provides approximately 650 GNSS-RO soundings per day [11].

TerraSAR-X/TanDEM-X: TerraSAR-X and TanDEM-X are a pair of German satellites managed by the German Aerospace Center. TerraSAR-X was launched in

[1]In this thesis, all data used for colocation analysis is from December 2020. At that time, one of the six COSMIC-2 satellites was at an altitude of 720 kilometers. The orbit has since been lowered to 520 kilometers.

Table 2.1: Public Sector GNSS-RO Missions since 2000. Missions highlighted in gray are used for colocation analysis in this thesis. Information in this table was compiled from the World Meteorological Organization (WMO) Observing Systems Capability Analysis and Review (OSCAR) Tool website [4].

Mission Name (# of Satellites)	**Launch Year**	**GNSS-RO Instrument**
Retired or Decayed		
CHAMP (1)	2000	BlackJack
SAC-C (1)	2000	GOLPE
SAC-D (1)	2011	ROSA
GRACE (2)	2002	BlackJack
FORMOSAT-3/COSMIC-1 (6)	2006	IGOR
KOMPSAT-5 (1)	2013	IGOR
C/NOFS (1)	2008	CORISS
Active		
MetOp-A/B/C (3)	2006, 2012, 2018	GRAS
TerraSAR-X, TanDEM-X (2)	2007, 2010	IGOR
OceanSat-2 (1)	2009	ROSA
FY-3C/D (2)	2013, 2017	GNOS
GRACE-FO (2)	2018	TriG
ROHP-PAZ (1)	2018	IGOR+
FORMOSAT-7/COSMIC-2 (6)	2019	TGRS
Sentinel-6A (1)	2020	GNSS-RO
Planned		
FY-3E/F/G/H (4)	2021, 2023, 2023, 2024	GNOS-2
MetOp-SG-A1/A2/A3 (3)	2024, 2031, 2037	RO
MetOp-SG-B1/B2/B3 (3)	2024, 2031, 2038	RO
Meteor-MP N1/N2 (2)	2025, 2026	ARMA-MP
Sentinel-6B (1)	2025	GNSS-RO

2007, with TanDEM-X following in 2010. Each satellite has an orbital inclination of 97.44° and an altitude of 514 kilometers. The satellites carry the Integrated GPS and Occultation Receiver (IGOR) instrument, which receives signals from the GPS global navigation constellation. TerraSAR-X provides approximately 175 GNSS-RO soundings per day, while TanDEM-X provides around 100 GNSS-RO soundings per day [6].

ROHP-PAZ: ROHP-PAZ is a Spanish satellite jointly operated by the Spanish Institute of Space Sciences and the company Hisdesat. ROHP-PAZ is in a 97.4° inclination sun-synchronous orbit at an altitude of 514 kilometers. The satellite was launched in 2018 as a proof-of-concept mission; ROHP-PAZ includes the IGOR+ GPS receiver, the first ever GNSS-RO instrument to take measurements at two polarizations [3]. IGOR+ receives signals from the GPS global navigation constellation. ROHP-PAZ provides approximately 250 GNSS-RO soundings per day [6].

2.2 Cross-Track Scanning Microwave Radiometry

2.2.1 Cross-Track Scanning Microwave Radiometry Geometry

Microwave radiometry is a passive remote sensing technique used to profile atmospheric temperature and humidity. As a satellite with a cross-track scanning microwave radiometer onboard orbits the Earth, the antenna on the radiometer scans in the direction normal to the satellite's direction of travel. Each scan involves a full, 360° rotation of the instrument, viewing both the Earth and space. As the radiometer antenna views the Earth, it moves continuously but takes a number of discrete soundings which are symmetric about the nadir direction. The total number of soundings is dependent on the specific radiometer being used. As the radiometer antenna rotates so that it no longer views Earth and thus views deep space, it takes cold calibration measurements. Following the cold calibration, the instrument takes a warm calibration measurement using an internal calibration source [42]. A generalized scan sequence is shown in Figure 2-3.

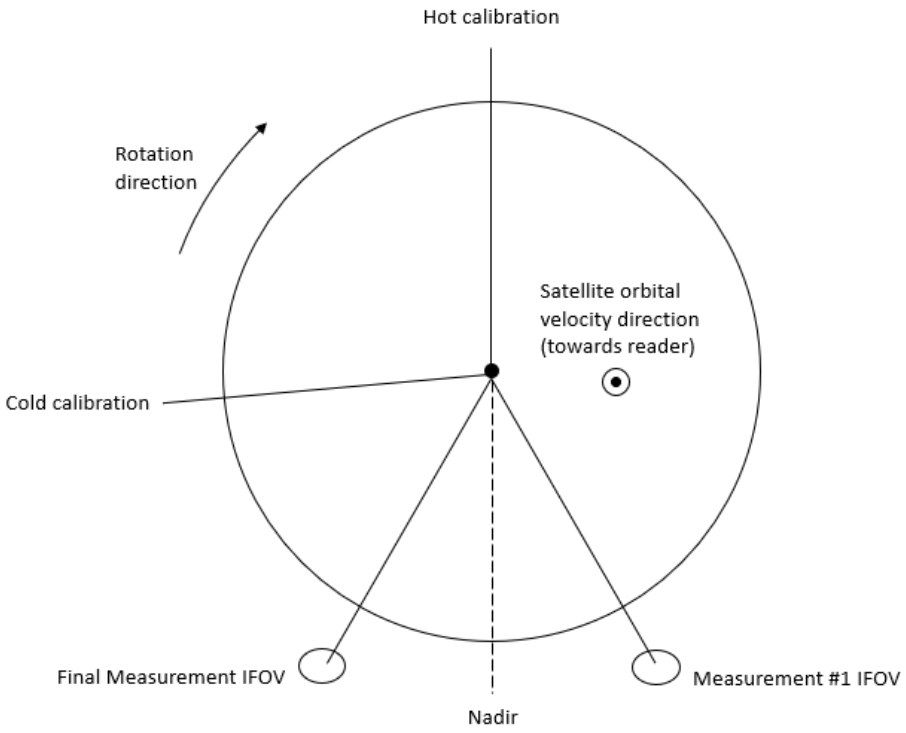

Figure 2-3: Generalized cross-track MWR scan sequence

2.2.2 Cross-Track Scanning Microwave Radiometry Atmospheric Science

Cross-track scanning microwave radiometers measure the intensity of microwaves using a number of different channels (corresponding to different frequencies). Measurements are taken by every channel during each discrete sounding throughout the MWR scan pattern. These measurements are used to calculate brightness temperature under the Rayleigh-Jeans approximation [37]. Atmospheric attenuation, mainly due to absorption by O_2 and H_2O molecules, impacts brightness temperature [25]. This attenuation is frequency dependent, and thus channels coinciding with absorption features can provide information about different atmospheric regions and properties. Frequencies near the peak of an absorption feature measure radiance in the upper atmosphere; frequencies away from the peak of an absorption feature measure radiance in the lower atmosphere [39]. For example, the absorption of electromagnetic (EM) radiation reaches a peak at 60 GHz due to attenuation by O_2 molecules. The

Advanced Technology Microwave Sounder (ATMS), an MWR instrument flown on several satellites, includes 12 channels that range from 51.76 GHz to 57.29 GHz. The channel at 51.76 GHz (furthest from the peak at 60GHz) observes the altitude corresponding with an atmospheric pressure of 950 hPa, while the channel at 57.29 GHz (closest to the peak at 60GHz) observes the altitude corresponding to an atmospheric pressure of 2 hPa [37]. Frequency ranges with attenuation dominated by O_2 molecules are optimal for temperature profiling, while frequency ranges with attenuation dominated by H_2O molecules are optimal for water vapor.

The relationship between different MWR channels and their sensitivity to different atmospheric altitudes is given via a weighting function. The weighting function describes the relative contribution of each atmospheric layer to the brightness temperature observed by a radiometer channel on a MWR instrument. At pressures where a channel's weighting function is near zero, atmospheric temperature and observed brightness temperatures have little correlation. The peak of the weighting function for a given channel represents the atmospheric layer that most influences the observed brightness temperature. Figure 2-4 depicts an example weighting function plot.

There are two types of microwave radiometers: sounders and imagers. Sounders have channels in opaque spectral regions to provide profiles of atmospheric temperature or water vapor, while imagers have channels in window spectral regions to provide information about cloud cover and precipitation [37].

2.2.3 Selected Cross-Track Scanning Microwave Radiometry Missions

Since the focus of this thesis is on finding colocated MWR measurements with temperature and water vapor profiles from radio occultation, only cross-track scanning MWR sounders (rather than imagers) are included. Table 2.2 provides a list of recent public sector missions with cross-track scanning MWR sounders onboard. Missions that are highlighted in the table are used for colocation analysis in this thesis. The performance assessment of colocation determination methods (Chapter 4) uses data

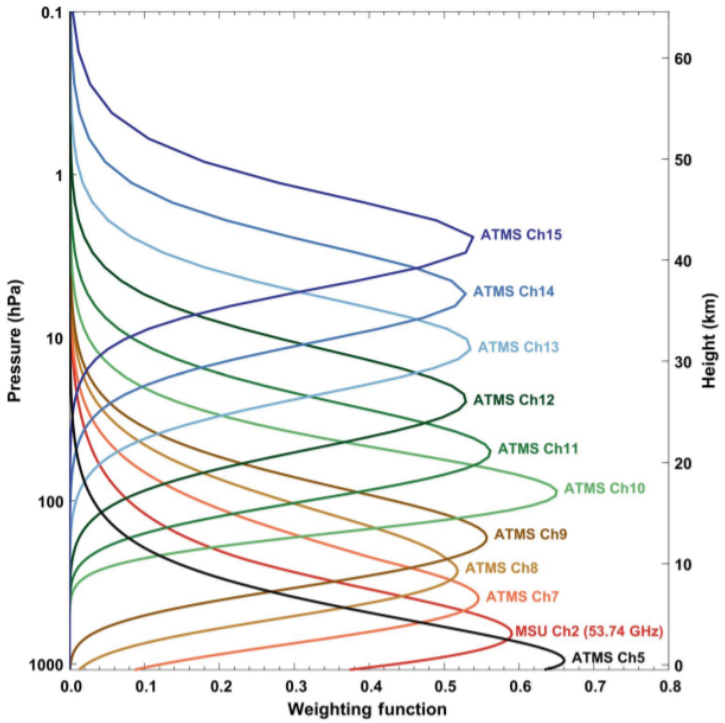

Figure 2-4: Weighting functions of ATMS channels 5-15 [43].

from the MetOp constellation and the NOAA-20 satellite. Analysis of colocations happening among active GNSS-RO and MWR missions (Chapter 5) considers the MetOp constellation and NOAA-20 satellite, and additionally includes the NOAA-18, NOAA-19, and Suomi-NPP satellites. The remaining active MWR missions listed in Table 2.2 are excluded due to retired or decayed instrumentation.

The orbital inclination, orbital altitude, Equatorial Crossing Time (ECT), and MWR payload for the selected MWR missions are given in Table 2.3. Each satellite is in a quasi-polar, sun-synchronous orbit. Three different MWR instruments are used across the selected satellites. A brief description of each instrument is included here:

Table 2.2: Public Sector Missions With Cross-Track Scanning MWR Sounders since 2000. Missions highlighted in gray are used for colocation analysis in this thesis. Information in this table was compiled from the WMO OSCAR website [4].

Mission (# of Satellites)	**Launch Year**	**MWR Sounding Instruments**
Retired or Decayed		
NOAA-16 (1)	2000	AMSU-A, AMSU-B
NOAA-17 (1)	2002	AMSU-A, MHS
FY-3A/3B (2)	2008, 2010	MWHS-1, MWTS-1
Active		
Aqua (1)	2002	AMSU-A, HSB
NOAA-18/19 (2)	2005, 2009	AMSU-A, MHS
MetOp-A/B/C (3)	2006, 2012, 2018	AMSU-A, MHS
Suomi-NPP (1)	2011	ATMS
Megha-Tropiques (1)	2011	SAPHIR
FY-3C/3D (2)	2013, 2017	MWHS-2, MWTS-2
NOAA-20 (1)	2017	ATMS
Planned		
TROPICS (7)	2021	TMS
FY-3E/F/H (3)	2021, 2023, 2024	MWTS-3, MWHS-2
MetOp-SG-A1/A2/A3 (3)	2024, 2031, 2037	MWS

Table 2.3: Orbital Parameters and MWR Payload for Selected MWR missions

Mission	**i (°)**	**Altitude (km)**	**Equatorial Crossing Time (local hour)**	**MWR Instrument**
MetOp-A	98.7	817	08:46 desc	AMSU-A[2], MHS[3]
MetOp-B	98.7	817	09:30 desc	AMSU-A, MHS
MetOp-C	98.7	817	09:30 desc	AMSU-A[4], MHS
NOAA-18	99.0	854	09:15 desc	AMSU-A, MHS[5]
NOAA-19	99.2	870	05:15 desc	AMSU-A[6], MHS[7]
NOAA-20	98.7	824	13:25 asc	ATMS
Suomi-NPP	98.7	833	13:25 asc	ATMS

AMSU-A: During each cross-track scan, AMSU-A takes 30 discrete measurements with a beamwidth of 3.3°. Each measurement is separated from its adjacent measurements by 3.33° along the scan direction, thus resulting in a maximum scan angle of 48.33° on either side of nadir. The footprint size from the beam varies throughout the course of the scan. The footprint size is 48 kilometers in diameter at nadir and 149 kilometers cross-track by 79 kilometers along-track at the maximum scan angle [16]. AMSU-A has three antennas which combined host 15 channels, spanning from 15 to 90 GHz. The instrument performs one full scan (360° rotation) every 8 seconds, 6 of which are spent viewing Earth [19].

MHS: The MHS instrument has 5 channels spanning from 83 to 190 GHz and takes 90 discrete measurements per scan. The instrument has a beam width of 1.11° and maximum scan angle of 49.44°. The footprint size is 17 kilometers in diameter at nadir and 52 kilometers cross-track by 27 kilometers along-track at the maximum scan angle [16]. The instrument performs one full scan (360° rotation) every $\frac{8}{3}$ seconds

[2]MetOp-A AMSU-A Channel 3 (50.3 GHz) and Channel 7 (54.95 GHz) are noisy [4]
[3]The MetOp-A MHS Channel 2 (157.0 GHz) is no longer functional [4]
[4]MetOp-C AMSU-A Channel 3 (50.3 GHz) is noisy [4]
[5]NOAA-18 MHS was turned off in 2016 due to a sequence of problems [4]
[6]NOAA-19 AMSU-A Channel 8 (55.5 GHz) is noisy [4]
[7]NOAA-19 MHS Channel 3 (183.311 ± 1.0 GHz) is noisy [4]

[19]. On the MetOp, NOAA-18, and NOAA-19 satellites, all MHS measurements are colocated with AMSU-A measurements [44].

ATMS: ATMS builds off heritage from the AMSU-A and MHS instruments, serving to provide similar channel coverage with one instrument instead of two [28]. ATMS has 22 channels, spanning from 23 to 183 GHz. The first 16 channels are designed mainly for sounding atmospheric temperatures; the remaining 6 are designed for water vapor sounding. The different channels have the same angular sampling angle of 1.11°, but vary in beam width. Channels 1-2 have a beam width of 5.2°, channels 3-16 have a beam width of 2.2°, and channels 17-22 have a beam width of 1.1° [38]. The maximum scan angle of the instrument is 52.725° relative to nadir. The footprint diameters for the different beam widths of 5.2°, 2.2°, and 1.1° are 75 kilometers, 32 kilometers, and 16 kilometers respectively at nadir. These sizes increase to 323 kilometers cross-track by 141 kilometers along-track, 137 kilometers cross-track by 60 kilometers along-track, and 64 kilometers cross-track by 30 kilometers along-track respectively at the maximum scan angle [27]. One full scan (360° rotation) is completed every $\frac{8}{3}$ seconds, 1.73 seconds of which are spent viewing Earth. ATMS takes 96 discrete measurements symmetric about nadir per scan. [34].

Chapter 3

Methods for Colocation Determination

Novel colocation determination methods are developed as tools to efficiently approximate the colocations found using "brute force." The mathematical theory behind the novel and "brute force" colocation determination methods is provided in this chapter. The next chapter applies all methods to real GNSS-RO and MWR data and compares the colocation outputs to validate the novel methods.

3.1 Overview of Methods

Two novel colocation methods are developed: one that is only applicable to MWR satellites in sun-synchronous orbits, and one that is applicable to MWR satellites in any orbit. The former was developed as a simple, sub-case of the latter. A sun-synchronous orbit can be described by just four values: local time of the ascending node, time of passage of the ascending node, inclination, and altitude. For the purpose of looking at colocated occultations on a time scale of several days, each of these values can be assumed to be constant. Non sun-synchronous orbits require additional orbital parameters, such as the Right Ascension of the Ascending Node (RAAN) and the mean motion, to characterize the orbit. These values cannot be assumed to be constant, thus making the task of developing a rotational transformation more com-

plex. A rotational method that considers sun-synchronous MWR orbits is developed first and then expanded upon to include all MWR orbits.

This chapter presents all three methods for finding colocations between cross-track scanning MWR soundings and GNSS-RO measurements:

- Rotational Transformation Colocation Determination - Sun-Synchronous (RTCD-SS)
- Rotational Transformation Colocation Determination - Generalized (RTCD-G)
- Brute Force Colocation Determination (BFCD)

Each method checks to see if the GNSS-RO and MWR measurements are 1) spatially colocated and 2) temporally colocated. If both are true, the GNSS-RO and MWR measurements are considered colocated.

3.2 Rotational Transformation Colocation Determination - Sun-Synchronous (RTCD-SS)

The consistent nature of cross-track scanning MWR sounding patterns is leveraged to produce an efficient algorithm to find colocated GNSS-RO and MWR soundings. Many MWR satellites are in polar, sun-synchronous orbits in order to enable daily global coverage. An example of daily coverage by a polar, cross-track scanning MWR satellite is shown in Figure 3-1. By mapping the location and times of a GNSS-RO sounding into a coordinate system natural to a cross-track scanning MWR satellite, the computational expense of finding GNSS-RO/MWR colocations is greatly reduced. The following colocation determination method is simplified to assume that the MWR satellite is in a sun-synchronous orbit. This method will be referred to as the Rotation Transformation Colocation Determination - Sun-Synchronous (RTCD-SS) method.

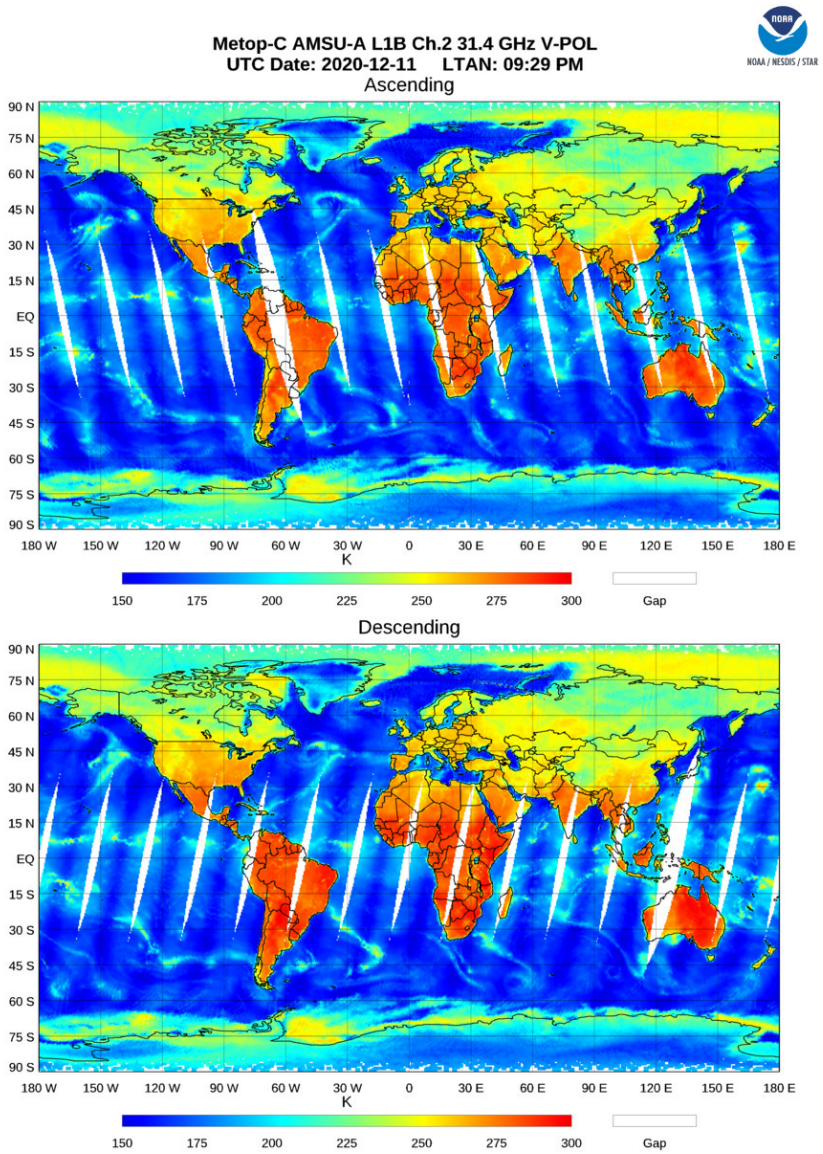

Figure 3-1: Example daily coverage by a polar, sun-synchronous, cross-track scanning MWR satellite. MetOp-C AMSU-A Channel 2 Level 1b data from 11 December 2020 is shown. The white in the image shows gaps in observations between scanning swaths [1].

3.2.1 Spatial Colocation

Radio occultation locations are initially defined in an Earth-centered coordinate system, where the x and y axes lie in Earth's equatorial plane and the z axis lies along Earth's spin axis (as shown in Figure 3-2a). The x axis is defined such that the axis always points to the sun's location projected onto Earth's equatorial plane from the ecliptic plane. This frame will be referred to as the Earth-Centered Radio Occultation (EC-RO) frame. Given the longitude λ_j, the latitude ϕ_j, and the time t_j, the position vector $\vec{r_j}$ of the j$^{\text{th}}$ occultation in the EC-RO frame becomes:

$$\vec{r_j} = \begin{bmatrix} \cos\left(\lambda_j + \Omega t_j\right)\cos(\phi_j) \\ \sin\left(\lambda_j + \Omega t_j\right)\cos(\phi_j) \\ \sin(\phi_j) \end{bmatrix} \tag{3.1}$$

where Ω is the solar-fixed spin rate of the Earth in radians per hour, $\frac{2\pi}{24}$. The addition of the Ωt_j term to the longitude in the x and y coordinates ensures that coordinate system measures longitudinal distance from the sun, rather than the distance from the vernal equinox (as is the case in the Earth-Centered Inertial coordinate system) or the prime meridian (as is the case in the Earth-Centered Earth-Fixed coordinate system).

This position vector $\vec{r_j}$ is rotated into the natural coordinate system of the MWR satellite, where the x axis lies along the line of nodes of the MWR satellite orbit, the z axis points along the angular momentum vector of the MWR satellite, and the y axis completes the coordinate system such that $\hat{x} \times \hat{y} = \hat{z}$. The position vector in the natural MWR frame for the j$^{\text{th}}$ occultation will be denoted as $\vec{\rho_j}$, where:

$$\vec{\rho_j} = \begin{bmatrix} \rho_{j,x} \\ \rho_{j,y} \\ \rho_{j,z} \end{bmatrix} \tag{3.2}$$

The transformation from the position vector in the EC-RO frame $\vec{r_j}$ to the position vector in the natural MWR satellite frame $\vec{\rho_j}$ requires two rotations, where i is the inclination of the MWR satellite and τ_N is the solar time at which the MWR satellite

crosses through the ascending node:

$$\vec{\rho_j} = \begin{bmatrix} 1 & 0 & 0 \\ 0 & \cos i & \sin i \\ 0 & -\sin i & \cos i \end{bmatrix} \begin{bmatrix} \cos(\Omega\tau_N) & \sin(\Omega\tau_N) & 0 \\ -\sin(\Omega\tau_N) & \cos(\Omega\tau_N) & 0 \\ 0 & 0 & 1 \end{bmatrix} \vec{r_j} \tag{3.3}$$

The coordinate system is first rotated by angle i about its x axis such that the z axis is perpendicular to the orbital plane of the MWR satellite. This rotation is shown in Figure 3-2b. The system is then rotated by $\Omega\tau_N$ about its z axis to align the x axis with the ascending node of the MWR satellite orbit. This rotation is shown in Figure 3-2c.

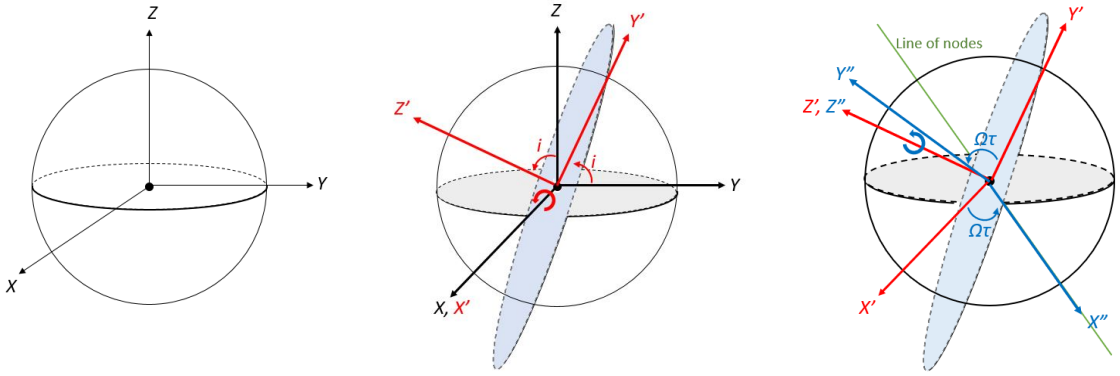

(a) Initial Coordinate System (b) Rotation 1 (c) Rotation 2

Figure 3-2: Coordinate system rotation to map the locations of GNSS-RO occultations in the EC-RO frame into the natural coordinate system of a sun-synchronous MWR satellite. Earth's equatorial plane is shown in gray and the orbital plane of the MWR satellite is shown in blue.

Now that the occultations of the GNSS-RO satellite are defined in the natural coordinate system of the MWR satellite, checking for spatial colocations is simple. To determine if the GNSS-RO occultation falls within the cross-track scan of the MWR satellite, the maximum displacement of the MWR scan on the Earth's surface measured from the sub-spacecraft location must be calculated. This maximum displacement, denoted by ds, is found using the Law of Sines. As can be seen in Figure 3-3, the maximum scan angle ξ_m, the satellite altitude h, the radius of the Earth R_E, and the angle θ are related such that:

$$\frac{R_E + h}{\sin\theta} = \frac{R_E}{\sin\xi_m} \tag{3.4}$$

Rearranging, it follows that:

$$\theta = \sin^{-1}\left(\frac{R_E + h}{R_E}\sin\xi_m\right) \tag{3.5}$$

Note that θ can take on two values, as the arcsin term produces two possible angles. As the value for θ at the tangent point is 90°, and thus θ must be $\geq 90°$, the larger value for θ is used. ds is solved for using the Triangle Angle Sum Theorem:

$$ds = 180 - \sin^{-1}\left(\frac{R_E + h}{R_E}\sin\xi_m\right) - \xi_m \tag{3.6}$$

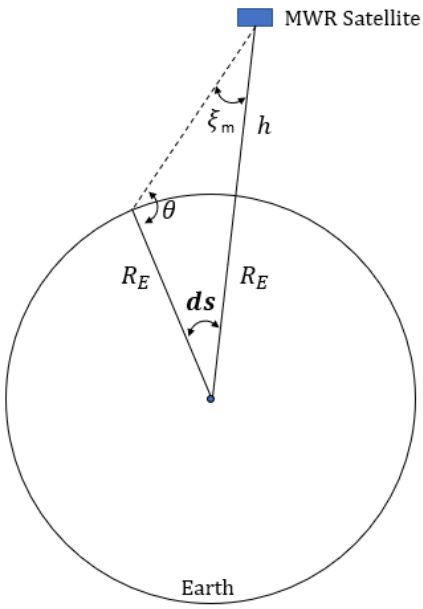

Figure 3-3: Cross-track scanning MWR satellite geometry.

Given this formulation, the coordinates of the GNSS-RO sounding can be translated back to spherical coordinates, where $\sin^{-1}(\rho_{j,z})$ relates to the cross-track scan of the MWR satellite and $u_j = \tan^{-1}(\rho_{j,y}, \rho_{j,x})$ is the "argument of latitude" of the GNSS-RO sounding (the argument of latitude the MWR satellite would have if and

when it scanned the GNSS-RO location). The GNSS-RO and MWR measurements are spatially colocated if the following inequality holds true:

$$|\sin^{-1}\rho_{j,z}| < |ds| \tag{3.7}$$

3.2.2 Temporal Colocation

To determine if GNSS-RO and MWR measurements are temporally colocated, the time of passage through the ascending node for the MWR satellite for the day of interest τ must be computed via the following equation:

$$\tau = t_E - (\omega + M)/n \tag{3.8}$$

The Two-Line Element (TLE) data for the MWR satellite provides the epoch t_E, the argument of perigee ω, the mean anomaly M, and the mean motion n that are used to calculate τ. The GNSS-RO and MWR measurements are temporally colocated if the following inequality, where Δt is the time tolerance for colocation and t_j is the time of the occultation, holds true:

$$\cos(u_j - n(t_j - \tau)) > \cos(n(\Delta t)) \tag{3.9}$$

3.3 Rotational Transformation Colocation Determination - Generalized (RTCD-G)

To generalize the RTCD-SS method to apply to all MWR satellites regardless of orbit, the transformation is changed to account for orbital nodal regression and apsidal precession. This method will be referred to as the Rotation Transformation Colocation Determination - Generalized (RTCD-G) method.

3.3.1 Spatial Colocation

To begin, radio occultation locations are defined in an ECEF coordinate system. The origin of the coordinate system is at the Earth's center, the x axis lies on the equatorial plane and points towards the prime meridian, the z axis runs along the Earth's spin axis pointing North, and the y axis completes the coordinate system such that $\hat{x} \times \hat{y} = \hat{z}$. Given the longitude λ_j, the latitude ϕ_j, and the time t_j, the position vector $\vec{r_j}$ of the j$^{\text{th}}$ occultation in ECEF coordinates is:

$$\vec{r_j} = \begin{bmatrix} \cos(\lambda_j)\cos(\phi_j) \\ \sin(\lambda_j)\cos(\phi_j) \\ \sin(\phi_j) \end{bmatrix} \tag{3.10}$$

This position vector must next be converted into a True Equator Mean Equinox (TEME) coordinate system. TEME is an inertial coordinate system similar to the Earth-Centered Inertial (ECI) coordinate system [2]. In the ECI coordinate system, the x axis lies on the equatorial plane and points towards the vernal equinox, the z runs along the Earth's rotational axis pointing North, and the y is orthogonal to the other axes such that the right hand rule holds. However, Earth's rotation axis and direction of the vernal equinox are not truly constant. The TEME coordinate system takes into account variations in these axes over time. In the TEME system, the x axis points towards the mean vernal equinox at the current epoch, the z axis points towards the true rotation axis at the current epoch, and the y axis completes the coordinate system such that $\hat{x} \times \hat{y} = \hat{z}$ [2]. This coordinate transformation is complex as it depends on the Earth's position at a specific epoch and is best performed using computational tools such as Python's *Astropy*. The new position vector $\tilde{r}_j$ in TEME coordinates becomes:

$$\tilde{r}_j = \begin{bmatrix} \tilde{r}_{j,x} \\ \tilde{r}_{j,y} \\ \tilde{r}_{j,z} \end{bmatrix} \tag{3.11}$$

The coordinates of the GNSS-RO occultation can now be translated back to spherical coordinates. The inertial latitude $\tilde{\theta}_j$ of the occultation and the inertial longitude $\tilde{\lambda}_j$

of the occultation are computed as such:

$$\tilde{\theta}_j = \sin^{-1}(\tilde{r}_{j,z}) \tag{3.12}$$

$$\tilde{\lambda}_j = \tan^{-1}(\tilde{r}_{j,y}, \tilde{r}_{j,x}) \tag{3.13}$$

The inertial latitude and inertial longitude can now be rotated into the natural coordinate system of the MWR satellite, where the x axis lies along the line of nodes of the MWR satellite orbit, the z axis points along the angular momentum vector of the MWR satellite, and the y axis completes the coordinate system such that $\hat{x} \times \hat{y} = \hat{z}$. The rotational transformation, given the inclination i and the RAAN Ω of the MWR satellite, is:

$$\tilde{\rho}_j = \begin{bmatrix} 1 & 0 & 0 \\ 0 & \cos i & \sin i \\ 0 & -\sin i & \cos i \end{bmatrix} \begin{bmatrix} \cos\left(\tilde{\lambda}_j - \Omega(t_j)\right)\cos(\tilde{\theta}_j) \\ \sin\left(\tilde{\lambda}_j - \Omega(t_j)\right)\cos(\tilde{\theta}_j) \\ \sin(\tilde{\theta}_j) \end{bmatrix} \tag{3.14}$$

The RAAN $\Omega(t_j)$ of the MWR satellite is approximated using:

$$\Omega(t_j) = \Omega_{epoch} + \dot{\Omega} \cdot (t_j - t_{epoch}) \tag{3.15}$$

Ω_{epoch} is the RAAN corresponding to the closest time epoch t_{epoch} (provided by a TLE file) proceeding time t_j of the occultation. The rate of change of RAAN, $\dot{\Omega}$ is given by:

$$\dot{\Omega} = -\frac{3}{2} n J_2 \left(\frac{R_E}{\rho}\right)^2 \cos i \tag{3.16}$$

where n is the mean motion of the MWR satellite, J_2 is the gravity coefficient corresponding to the Earth's equatorial bulge, R_E is the Earth's equatorial radius, p is the semi-latus rectum of the MWR satellite's orbit, and i is the inclination of the MWR satellite's orbit. From here, the check for spatial colocation is essentially identical to the RTCD-SS method. Recall ds, the maximum displacement of the MWR scan on the Earth's surface measured from the sub-spacecraft location, calculated in Equation

3.6. The GNSS-RO and MWR measurements are spatially colocated if the following inequality holds:

$$|\sin^{-1}\tilde{\rho}_{z,j}| < |ds| \tag{3.17}$$

3.3.2 Temporal Colocation

The temporal colocation is almost identical to that of the RTCD-SS method. The time of passage τ through the ascending node for the MWR satellite for the day of interest is computed using Equation 3.8.

The "argument of latitude" of the occultation (the argument of latitude the MWR satellite would have if and when it scanned the occultation location) is defined as $\tilde{u}_j = \tan^{-1}(\tilde{\rho}_{j,y}, \tilde{\rho}_{j,x})$. As with the RTCD-SS method, the GNSS-RO and MWR measurements are temporally colocated if the inequality, where Δt is the time tolerance for colocation and t_j is the time of the occultation, holds true:

$$\cos(\tilde{u}_j - n(t_j - \tau)) > \cos(n(\Delta t)) \tag{3.18}$$

3.4 Brute Force Colocation Determination (BFCD)

The typical method used to find colocations in previous studies will be referred to as the Brute Force Colocation Determination (BFCD) method. The BFCD method involves exhaustively searching through each occultation and each MWR sounding to check if the measurements are colocated.

3.4.1 Spatial Colocation

A GNSS-RO measurement with latitude θ_j and longitude λ_j and an MWR measurement with latitude θ_m and longitude λ_m are spatially colocated if the following inequality holds:

$$\sqrt{(\lambda_j - \lambda_m)^2(\cos\theta_j)^2 + (\theta_j - \theta_m)^2} < \Delta d \tag{3.19}$$

where Δd is the spatial tolerance. This equation is very similar to the simple Euclidean distance formula, but with an additional cosine term. The multiplication by $(\cos\theta_j)^2$ accounts for the effect that two points separated by 1° in longitude at the equator are much farther apart in reality than two points separated by 1° in longitude at the Arctic Circle.

3.4.2 Temporal Colocation

For a GNSS-RO occultation with time t_j and an MWR sounding at time t_m, the measurements are temporally colocated if the following inequality holds:

$$|t_j - t_m| < \Delta t \tag{3.20}$$

THIS PAGE INTENTIONALLY LEFT BLANK

Chapter 4

Performance Assessment of Rotational Methods for Colocation Determination

The mathematical theory of the Rotational Transformation Colocation Determination (RTCD) methods described in Chapter 3 is validated in three ways:

1. Applying the RTCD-SS rotation matrices to cross-track scanning MWR satellite data rather than GNSS-RO data and confirming that the results are as expected;

2. Comparing RTCD-G and RTCD-SS results with sun-synchronous MWR satellites and confirming that the outputs are the same;

3. Assessing the performance of the RTCD-G method through comparison to the BFCD method.

All methods are implemented in Python 3.7 using data from NOAA-20, COSMIC-2, and MetOp-C (see Section 4.1). The code to implement the BFCD algorithm is given in Appendix A.1, and the code to implement the RTCD-G and RTCD-SS algorithms is given in Appendix A.2. The code to define satellite objects is given in Appendix A.3, examples of instantiated satellite objects are given in Appendix A.4, and the constants used throughout the code are given in Appendix A.5. The

Table 4.1: Colocation Criteria

Criteria	**Maximum Distance**
Temporal (Δt)	10 minutes
Spatial (Δd)	150 kilometers

Table 4.2: Constants Used by Colocation Determination Code

Constant	**Value**
J2 Perturbation, J_2 $[unitless]$	$1.08262668 \times 10^{-3}$
Earth Radius, R_E $[km]$	6371
Earth Solar Fixed Spin Rate, Ω $[\frac{radians}{hour}]$	0.26179939
Earth Standard Gravitational Parameter, μ $[\frac{m^3}{s^2}]$	$3.986004418 \times 10^{14}$

constants used throughout the code are also given in Table 4.2. The criteria for a colocation is given in Table 4.1; measurements must always be within 10 minutes and 150 kilometers of one another.

4.1 Implementation

4.1.1 Radio Occultation Data

Radio occultation data for all GNSS-RO missions considered in this thesis (COSMIC-2, MetOp-A, MetOp-B, MetOp-C, TerraSAR-X, TanDEM-X, and ROHP-PAZ) are available through the COSMIC Data Analysis and Archive Center (CDAAC) run by the University Corporation for Atmospheric Research (UCAR) [7]. GNSS-RO Level 2 data in the form of atmPrf (atmospheric profile) files are used. Each occultation is an individual Network Common Data Form (netCDF) file, downloadable in zipped files organized by day of the year.

The location and time of each occultation must be known for colocation determination. Though an entire occultation event lasts 1-2 minutes, a single occultation time (referred to as the "occultation point") is assigned to the atmospheric profile retrieved from the occultation. CDAAC's processed data defines the occultation point as the tangent point of the ray connecting the GNSS satellite in MEO to the GNSS receiver satellite in LEO for which L1 (1575.42 MHz) excess phase is equal to 500

Table 4.3: MWR Satellite NORAD Catalogue Numbers

Satellite Name	**NORAD Catalogue Number**
MetOp-A	29499
MetOp-B	38771
MetOp-C	43689
NOAA-18	28654
NOAA-19	33591
NOAA-20	43013
Suomi-NPP	37849

meters [32]. The latitude and longitude assigned to the occultation point are the latitude and longitude of the perigee point at the occultation point. The occultation point latitude and longitude are given as global attributes *lat* and *lon* in the netCDF occultation files. The netCDF occultation files include the starting time of the occultation event, the ending time for the occultation event, and the time offset from the starting time of the occultation event to the occultation point time, corresponding to the netCDF file global variables *start_time*, *stop_time*, and *occpt_offset*. The time of the occultation point is defined as the addition of the start time and the offset time, $start\_time + occpt\_offset$.

4.1.2 Cross-Track Microwave Radiometry Data

Two-Line Element (TLE) sets are needed to determine colocations using the RTCD-SS method and RTCD-G method. TLE files for all MWR satellites considered in this thesis (MetOp-A, MetOp-B, MetOp-C, NOAA-18, NOAA-19, NOAA-20, and Suomi-NPP) are available through the CelesTrak website. The North American Aerospace Defense Command (NORAD) catalogue number of a satellite must be known in order to request TLE data for that satellite. The NORAD catalogue number for each MWR satellite considered in this thesis is given in Table 4.3.

The BFCD method requires comprehensive MWR datasets. NOAA-20 data in the form of ATMS Sensor Data Record (SDR) Ellipsoid Geolocation files are available through the NOAA Comprehensive Large Array-data Stewardship System (CLASS) [8]. The MWR data for a single day is spread throughout 180 Hierarchical Data

Format 5 (H5) files. The time and location of each MWR sounding must be known for colocation determination using BFCD. The latitude and longitude of each sounding are defined as the latitude and longitude of the ATMS Channel 17 beam position center for that sounding [26]. These variables are found within the H5 files at *All_Data/ATMS-SDR-GEO_All/Longitude* and *All_Data/ATMS-SDR-GEO_All/Latitude*. The H5 files give the starting time and mid time of each scan, rather than a specific time for each sounding. As a result, the time of each sounding within a scan is approximated to be the mid time of that scan. The mid time variable is found within the H5 file at *All_Data/ATMS-SDR-GEO_All/MidTime*.

MetOp-C AMSU-A data is available through the EUMETSAT Data Centre Earth Observation Portal. MetOp-C AMSU-A Global Data Set (GDS) Level 1B data can be ordered from this portal in the form of netCDF files. The data for a single day is spread throughout 14-15 files. The latitude of the sounding is given in degrees North under the netCDF variable *lat* and the longitude of the sounding is given in degrees East under the netCDF variable *lon*. The netCDF files include the time associated with the first and last soundings in each scan (netCDF variables *record_start_time* and *record_stop_time*), rather than a specific time for each sounding. As a result, the time of each sounding within a scan is approximated to be the midpoint *mid_time* of the scan:

$$mid\_time = record\_start\_time + \frac{|record\_stop\_time - record\_start\_time|}{2} \quad (4.1)$$

.

4.2 Validation and Accuracy of Rotational Methods

4.2.1 Validation of RTCD-SS Using MWR Data

To verify the correctness of the RTCD-SS rotation matrices defined in Equation 3.3, the RTCD-SS method is implemented using MWR data. If the rotation matrices are

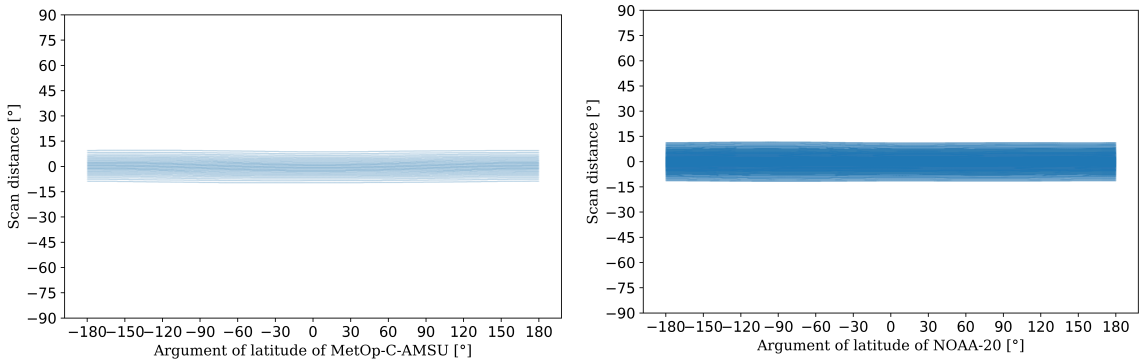

(a) Rotated MetOp-C AMSU Data (b) Rotated NOAA-20 ATMS Data

Figure 4-1: Validation of RTCD-SS rotation matrices. The RTCD-SS algorithm is implemented using MWR data, rather than GNSS-RO data.

implemented correctly, all of the rotated MWR soundings should appear in a band that straddles the equator. To perform the rotation, Equation 3.3 becomes:

$$\rho_m = \begin{bmatrix} 1 & 0 & 0 \\ 0 & \cos i & \sin i \\ 0 & -\sin i & \cos i \end{bmatrix} \begin{bmatrix} \cos(\Omega\tau_N) & \sin(\Omega\tau_N) & 0 \\ -\sin(\Omega\tau_N) & \cos(\Omega\tau_N) & 0 \\ 0 & 0 & 1 \end{bmatrix} \begin{bmatrix} \phi_m \\ \lambda_m \\ t_m \end{bmatrix} \tag{4.2}$$

where ϕ_m is the latitude of the mth MWR sounding, λ_m is the longitude of the mth MWR sounding, and t_m is the time of the mth MWR sounding. In the new coordinate system, $\tan^{-1}(\rho_{m,y}, \rho_{m,x})$ is the the argument of latitude of the mth sounding and $\sin^{-1}(\rho_{m,z})$ is the cross-track scanning coordinate of the mth sounding. The cross-track scanning coordinate plotted as a function of the argument of latitude is shown for one day's worth of MetOp-C AMSU-A soundings in Figure 4-1a and one day's worth of NOAA-20 ATMS soundings in Figure 4-1b. As is expected, in this formulation all of the MWR soundings appear in a band that straddles the equator. The maximum scan distance for AMSU-A from the data shown in Figure 4-1a is 9.64°, which is close to the theoretical ds value of 9.23° calculated for AMSU-A. Similarly, the maximum scan distance for the ATMS instrument from the data shown in Figure 4-1a is 11.66°, which is close to the theoretical ds value of 11.42° calculated for ATMS.

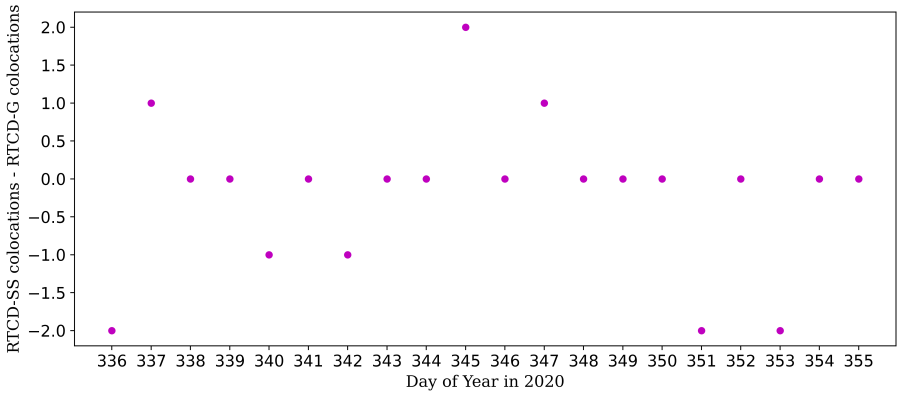

Figure 4-2: Comparison of RTCD-G and RTCD-SS methods for NOAA-20/COSMIC-2 Colocations from 1 December 2020 to 20 December 2020. RTCD-G finds an average of 132 colocations per day during this time period.

4.2.2 RTCD-SS and RTCD-G Comparison

Since RTCD-G is a generalized version of RTCD-SS, the two methods should produce the same output when a MWR satellite in a sun-synchronous orbit is used. This is verified by computing the number of colocations found between NOAA-20 and COSMIC-2 for 20 days using both the RTCD-G method and the RTCD-SS method. The difference in colocations found between the methods is shown in Figure 4-2. On the majority of the days, there is no difference between the two methods. Occasionally, there is a difference of 1-2 colocations found (relative to an average of 132 colocations found per day by RTCD-G during the period shown). These small differences are likely due to the simplified nature of the RTCD-SS method - any small variations in the RAAN of the MWR satellite that are ultimately corrected by orbital station-keeping are not captured. The RTCD-G method does capture these small variations. The almost identical performance of the two methods gives assurance that the RTCD-G method is implemented correctly.

4.2.3 RTCD-G and BFCD Comparison

To assess the performance of the RTCD-G and RTCD-SS methods, colocation outputs from the RTCD-G method are compared to colocation outputs from the BFCD

method. BFCD colocations are considered the true number of colocations. Colocations are found for 12 days of data, from 1 December 2020 through 14 December 2020. Colocations are found for four combinations of GNSS-RO and MWR satellites: NOAA-20/COSMIC-2, NOAA-20/MetOp-C GRAS, MetOp-C AMSU/COSMIC-2, and MetOp-C AMSU/MetOp-C GRAS.

RTCD-G Accuracy

The results (shown in Figure 4-3) demonstrate that RTCD-G consistently underestimates the amount of colocations found by the BFCD method. In Figure 4-3, the red dots indicating the number of RTCD-G colocations found are always below the blue dots indicating the number of BFCD colocations found, with the exception of two days of MetOp-C AMSU/COSMIC-2 colocations. The number of colocations found by the RTCD-G differs from those found by the BFCD method by an average of 14.3 colocations with a standard deviation of 9.8. The percent of colocated occultations found by RTCD-G differs from that found by BFCD by an average of 1.5% with a standard deviation of 2.0%.

Overall, RTCD-G provides a good "order-of-magnitude" estimate of the number of colocations found between MWR and GNSS-RO missions. Table 4.5 gives the average number of colocations found per day and the average percent of occultations that are colocated per day for each set of missions for each method. In general, RTCD-G mirrors the differences in colocations found by BFCD between the various mission combinations. Both methods find the highest percent of colocated occultations with the cohosted MetOp instruments, and the lowest percent with MetOp-C AMSU/COSMIC-2.

Disparities between the RTCD-G and BFCD method likely stem from two sources. First, the RTCD-G method assumes that the time of a colocation is the same time as the colocated GNSS-RO sounding, rather than the colocated MWR sounding. Using the GNSS-RO local time as the value for t_j in Equation 3.14 induces some error in the temporal colocation. The RTCD-G method will miss some colocations by failing the temporal colocation check when the two measurements are actually within 10 minutes

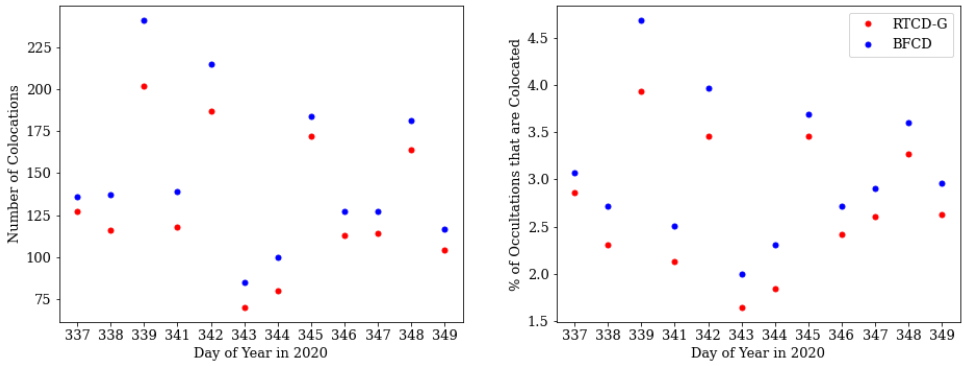

(a) NOAA-20/COSMIC-2

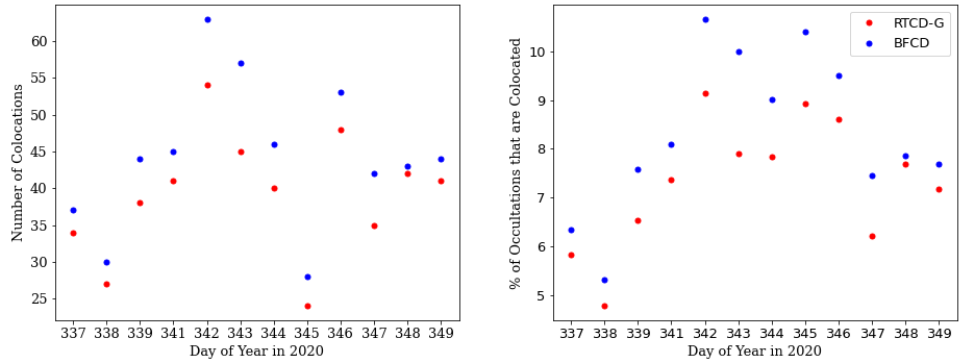

(b) NOAA-20/MetOp-C GRAS

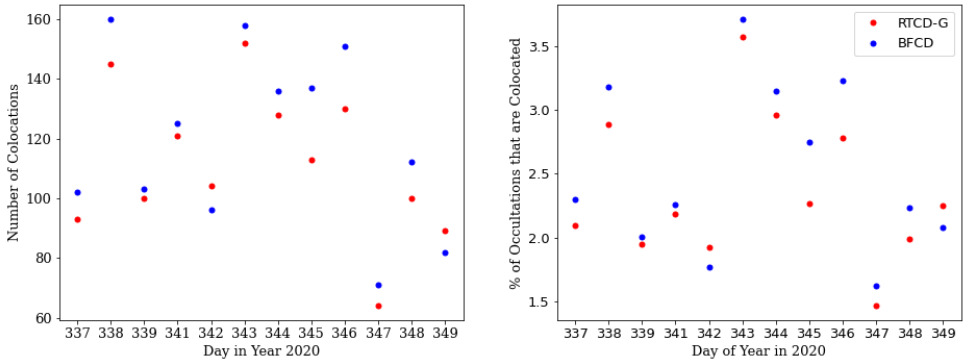

(c) MetOp-C AMSU/COSMIC-2

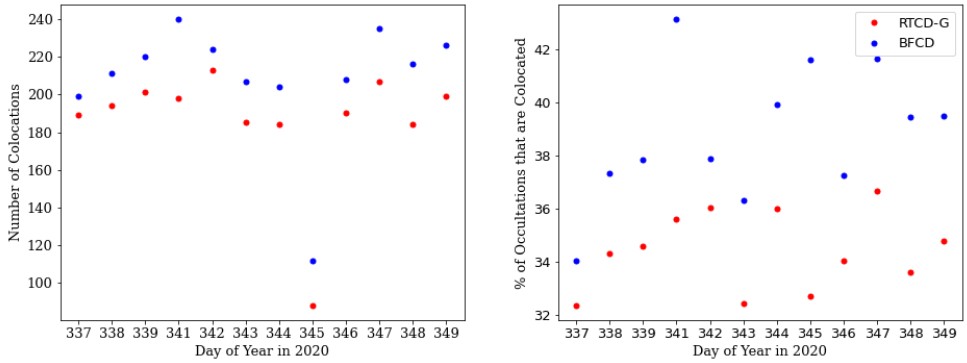

(d) MetOp-C AMSU/MetOp-C GRAS

Figure 4-3: Comparison of amount of colocations found by RTCD-G and BFCD methods over a 12 day period.

Table 4.4: Summary of colocations per day found by RTCD-G and BFCD for various mission combinations

	Avg Colocations/Day		Avg % Colocated Occultations	
	BFCD	RTCD-G	BFCD	RTCD-G
NOAA-20/COSMIC-2	149.1	130.6	3.1	2.7
NOAA-20/MetOp-C GRAS	44.3	39.1	8.3	7.3
MetOp-C AMSU/COSMIC-2	119.4	111.6	2.5	2.4
MetOp-C AMSU/MetOp-C GRAS	208.5	186.0	38.8	34.4

of one another. Second, the RTCD-G method spatial colocation check requires that the GNSS-RO occultation occur within the scanning pattern of the MWR satellite. However, the BFCD method is able to find colocations that are up to 150 kilometers outside of this scan pattern. The RTCD-G method misses some colocations when the GNSS-RO sounding is located just outside of the MWR satellite scan pattern. Colocations found by BFCD but missed by RTCD-G for day 337 of 2020 are shown in Figure 4-4.

Although the RTCD-G method underestimates the number of existing colocations, the colocations found by the RTCD-G method maintain a very similar latitudinal and longitudinal distribution to those found by the BFCD method. Figure 4-5 shows the locations of colocations found between MetOp-C AMSU and MetOp-C GRAS for a single day (day 337 of 2020). The distribution of colocations found by the two methods are similar, each finding almost no colocations in latitude range [-15°, 15°]. Both methods find the colocations spread throughout latitude ranges [-85°, -15°] and [15°, 85°]. Colocation distributions for the same day for MetOp-C AMSU and COSMIC-2 are shown in Figure 4-6. Both methods find colocations exclusively in the [-45°, 45°] range. The RTCD-G method finds peaks in colocations at around -15° and 20° that the BFCD method finds as well. Figure 4-7 shows the colocations found for day 337 between NOAA-20 and MetOp-C GRAS. This combination of missions produces another distinct-looking distribution of colocations. Both methods find very few colocations overall, and these colocations are found exclusively at latitudes less than -50° and greater than 50°. Finally, Figure 4-8 shows colocations found between NOAA-20 and COSMIC-2. Again, the two methods produce similar distributions.

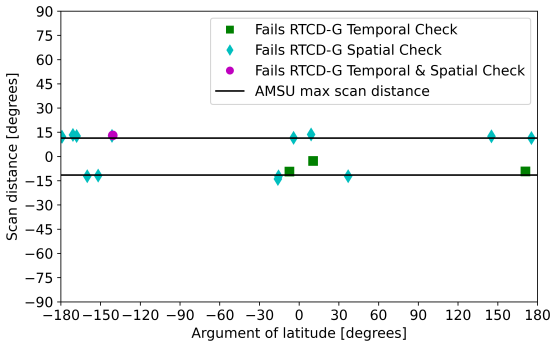

(a) NOAA-20/COSMIC-2

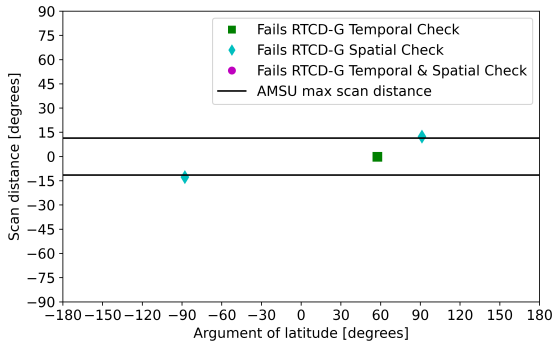

(b) NOAA-20/MetOp-C GRAS

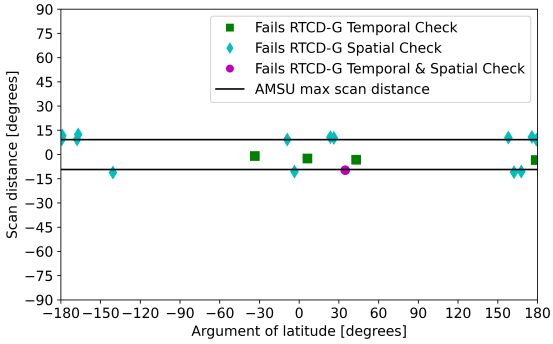

(c) MetOp-C AMSU/COSMIC-2

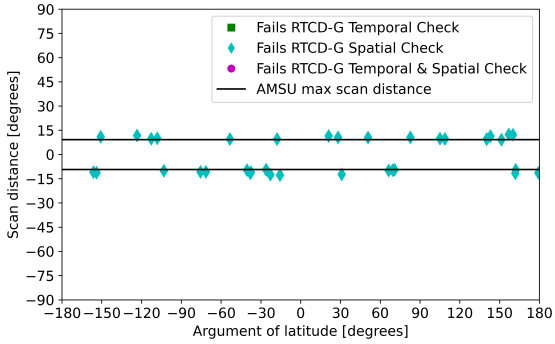

(d) MetOp-C AMSU/MetOp-C GRAS

Figure 4-4: Colocations found by BFCD but missed by RTCD-G for day 337 of 2020. Colocations that were not found because the RTCD-G temporal check (see Section 3.3.2) failed are shown in green, colocations that were not found because the RTCD-G spatial check (see Section 3.3.1) failed are shown in cyan, and colocations that were not found because both RTCD-G checks failed are shown in magenta.

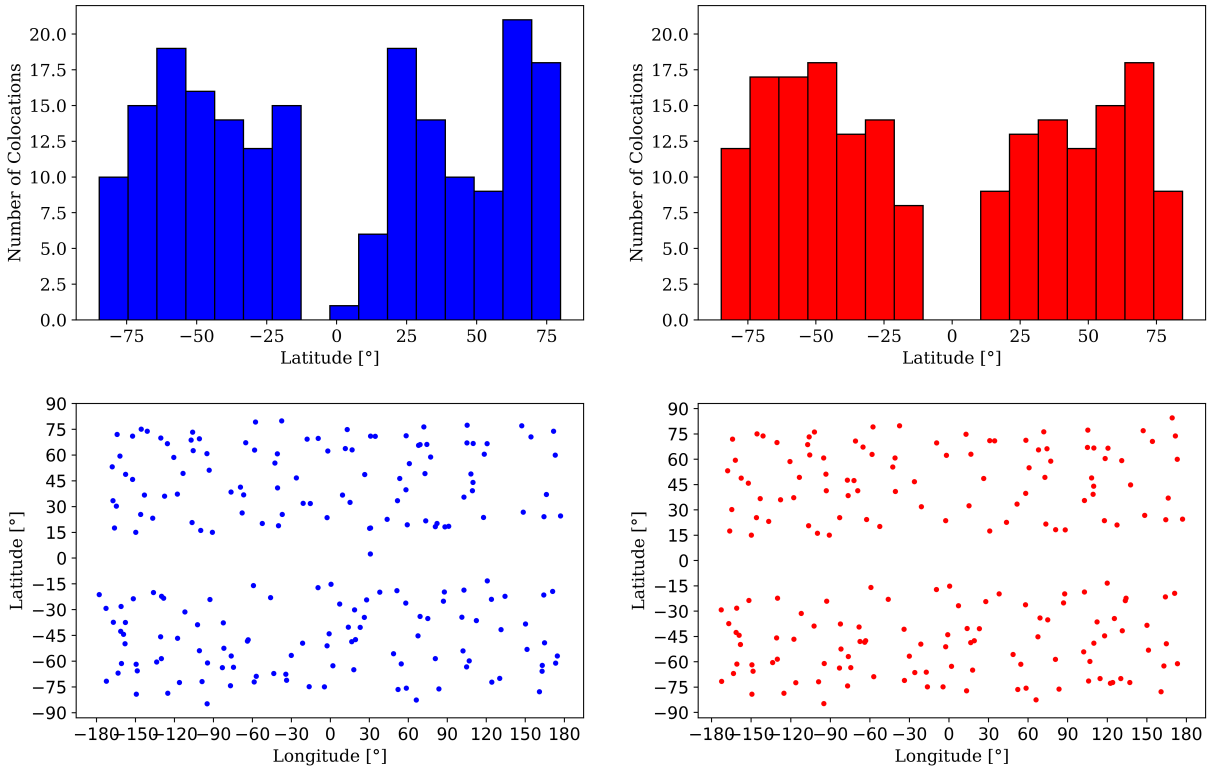

(a) BFCD (b) RTCD-G

Figure 4-5: Distribution of MetOp-C AMSU/MetOp-C GRAS colocations found by the BFCD and RTCD-G methods during day 337 of 2020. Measurements must be within 10 minutes and 150 kilometers of one another to be considered colocated.

Both methods find that the colocations are all located within the [-40°, 40°] range, with higher colocation densities near the equator.

The distribution of colocations looks quite different for the various combinations of MWR and GNSS-RO missions considered. The RTCD-G method is able to reflect such differences. The RTCD-G method finds colocations in the same range of latitudes as the BFCD method does, and finds nearly the same colocation densities within these ranges.

RTCD-G Speed

The time to compute colocations per day, averaged over the same 12 days of data, is recorded. The two methods are run in Python 3.7 on a Dell Latitude 7490 with 32 GB

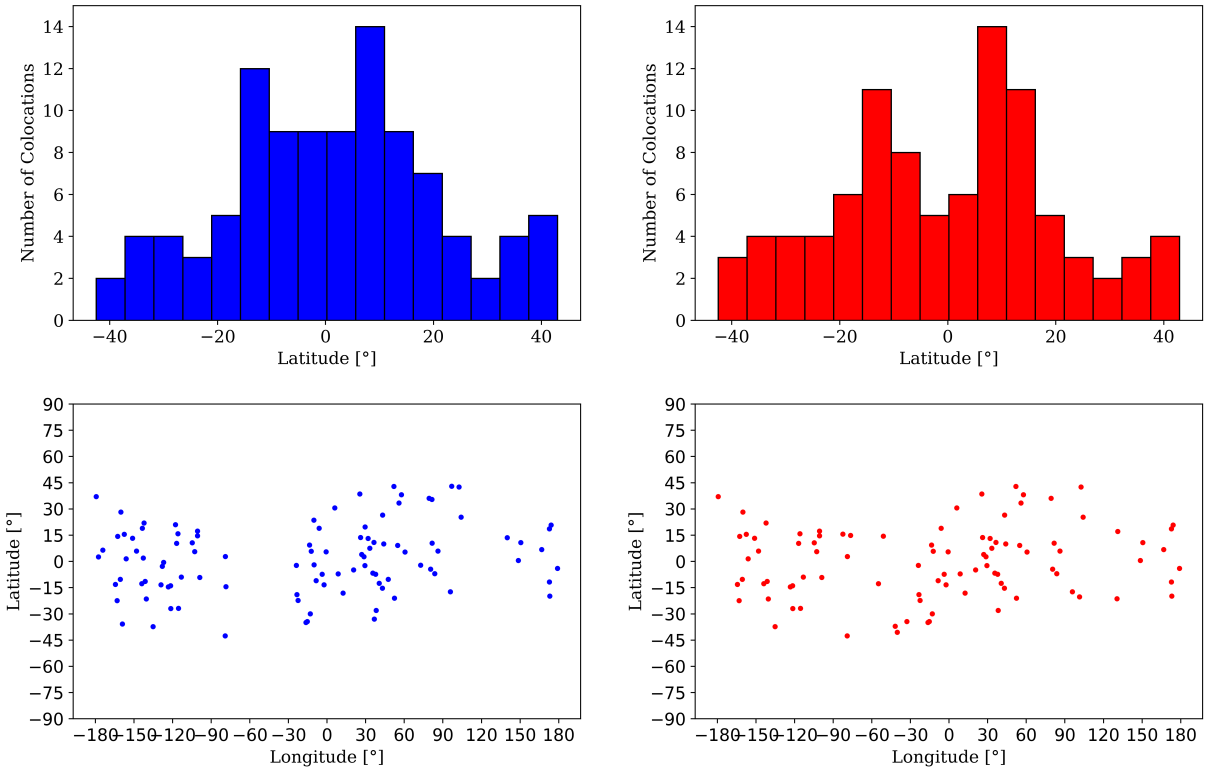

(a) BFCD (b) RTCD-G

Figure 4-6: Distribution of MetOp-C AMSU/COSMIC-2 colocations found by the BFCD and RTCD-G methods during day 337 of 2020. Measurements must be within 10 minutes and 150 kilometers of one another to be considered colocated.

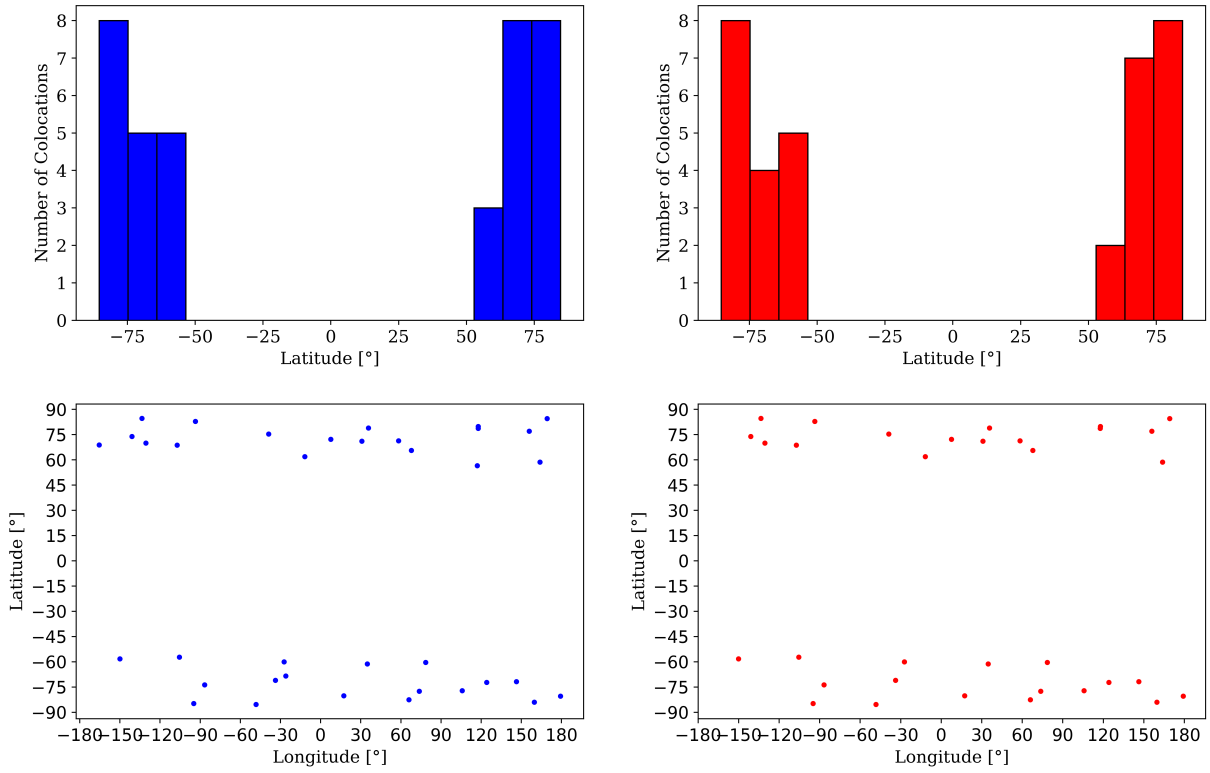

(a) BFCD (b) RTCD-G

Figure 4-7: Distribution of NOAA-20/MetOp-C GRAS colocations found by the BFCD and RTCD-G methods during day 337 of 2020. Measurements must be within 10 minutes and 150 kilometers of one another to be considered colocated.

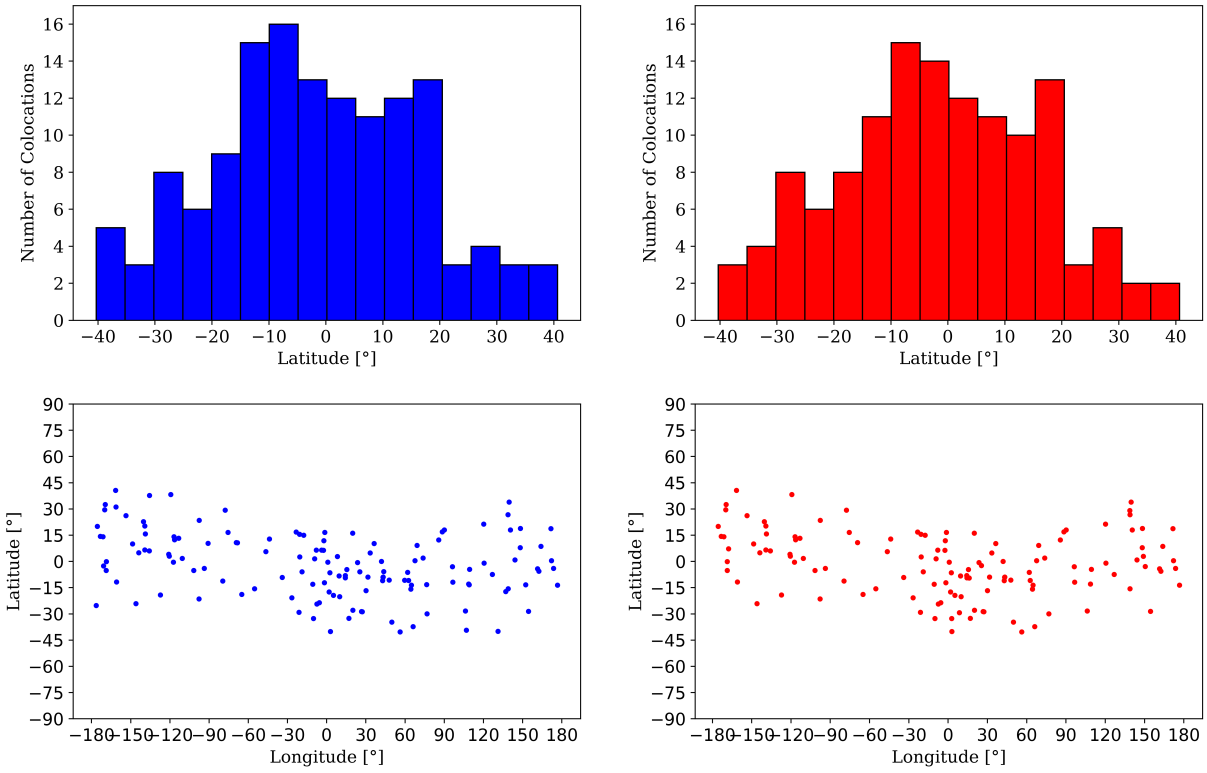

(a) BFCD (b) RTCD-G

Figure 4-8: Distribution of NOAA-20/COSMIC-2 colocations found by the BFCD and RTCD-G methods during day 337 of 2020. Measurements must be within 10 minutes and 150 kilometers of one another to be considered colocated.

Table 4.5: Time to compute colocations per day for BFCD and RTCD-G

	Avg Time to Compute Colocations/Day (minutes)	
	BFCD	RTCD-G
NOAA-20/COSMIC-2	13.4	0.427
NOAA-20/MetOp-C GRAS	1.53	0.046
MetOp-C AMSU/COSMIC-2	2.69	0.34
MetOp-C AMSU/MetOp-C GRAS	0.243	0.039

RAM and an Intel i7 processor with a clock speed of 1.9 GHz running Windows 10 Enterprise. The average times to compute colocations per day are listed in Table 4.5. The RTCD-G method always executes faster than the BFCD method. The RTCD-G method runs ∼32x faster for NOAA-20/COSMIC-2 colocations, ∼33x faster for NOAA-20/MetOp-C GRAS colocations, ∼8x faster for MetOp-C AMSU/COSMIC-2 colocations, and ∼6x faster for MetOp-C AMSU/MetOp-C GRAS colocations. Overall, RTCD-G runs ∼20x faster than BFCD on average.

THIS PAGE INTENTIONALLY LEFT BLANK

Chapter 5

Example RTCD-G Applications

5.1 Analysis of Existing Colocations

The RTCD-G method is first applied to survey the colocations that occur among active missions. 7 MWR satellites and 12 GNSS-RO satellites (6 of which make up the COSMIC-2 constellation) are considered. For each satellite in the MetOp constellation, only setting occultations are included due to the poor quality of rising occultations [35]. Colocations are found for 14 days in December 2020 and averaged to produce an estimate of colocations per day. Again, the criteria for measurements to be considered colocated are that the measurements be within 10 minutes and 150 kilometers of one another. Average colocations per day are given in Table 5.1. An average of 1297 colocations per day are found in total across the 7 MWR and 12 GNSS-RO satellites. The majority of colocations involve the COSMIC-2 constellation. 60% of all colocations involve the COSMIC-2 constellation, 33% involve the GRAS instruments on the MetOp constellation, and the remaining 7% result from TanDEM-X (TDX), TerraSAR-X (TSX), and PAZ.

The latitudinal and longitudinal distribution of colocations has little variation from day to day. The location of all colocations found during a single example day (day 339 of 2020) are shown in Figure 5-1. Colocation density is highest near the equator and lowest near the poles. The tropics (latitudinal range [-23.5°, 23.5°]) and subtropics (latitudinal ranges [-35°, -23.5°] and [23.5°, 35°]) are of particular

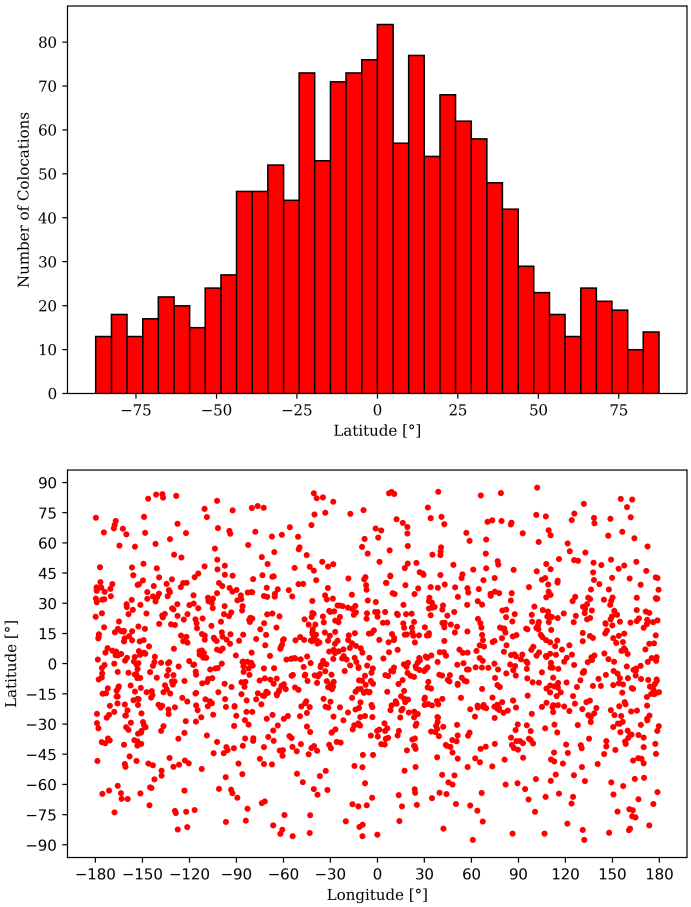

Figure 5-1: Distribution of all colocations among 7 active MWR satellites and 12 active GNSS-RO satellites found by the RTCD-G method during day 339 of 2020.

importance to weather prediction [20]. Of the 1297 colocations found on average, 543 (42%) are found in the tropics, 241 (18%) are found in the subtropics, and 513 (40%) are found outside of these regions.

5.2 Trailing COSMIC-2 Constellation

The RTCD-G method makes it possible to design future MWR missions to maximize colocations with GNSS-RO missions. Preliminary investigation of a constellation design that maximizes colocations with the COSMIC-2 constellation is performed. Possible colocations from a "trailing" MWR constellation are assessed since co-hosting

Table 5.1: Average GNSS-RO/MWR colocations per day among active missions estimated by RTCD-G

		RO Missions							
		COSMIC-2	MetOp-A	MetOp-B	MetOp-C	PAZ	TSX	TDX	
MWR Missions	NOAA-18	107.6	9.7	11.8	26.0	4.2	2.7	1.6	163.6
	NOAA-19	110.0	12.1	13.6	3.4	18.5	12.3	11.0	181.6
	NOAA-20	126.4	0.2	5.4	12.0	2.4	1.4	2.1	150.1
	Suomi-NPP	114.9	13.7	13.0	4.9	3.5	2.5	1.9	154.4
	MetOp-A	100.7	99.7	0.0	0.0	6.0	3.4	2.2	212.0
	MetOp-B	105.5	0.0	101.4	0.0	3.6	2.9	2.4	215.7
	MetOp-C	112.6	0.0	0.0	98.8	3.6	2.4	1.8	219.2
		778.4	135.4	145.1	145.1	41.9	27.6	23.0	

MWR instruments on the COSMIC-2 constellation is not possible. Other constellation architectures, such as one with satellites in similar orbits to the COSMIC-2 constellation but at higher altitudes may also serve to maximize the number of colocations with COSMIC-2. This "higher altitude" architecture is not explored in this thesis but should be investigated in future work (see Section 6.2).

MWR satellites are simulated to "trail" COSMIC-2 satellites by k seconds in time. The orbital period T of the COSMIC-2 satellite is calculated to identify the corresponding shift in argument of latitude. The orbital period is calculated using the following equation, where a is the semi-major axis of the COSMIC-2 satellite and μ_E is the standard gravitational parameter of the Earth:

$$T = 2\pi\sqrt{\frac{a^3}{\mu_E}} \tag{5.1}$$

If the COSMIC-2 orbit is assumed to be circular, the degrees of argument of latitude X that k seconds equates to is found using the following equation:

$$X = \frac{k}{T} \times 360 \tag{5.2}$$

COSMIC-2 TLE files with the argument of latitude shifted by X can be used with the RTCD-G method to simulate trailing MWR satellites. Six satellites are simulated, one to trail each of the six COSMIC-2 satellites. The simulated MWR satellites are named trail_44343, trail_44349, trail_44350, trail_44351, trail_44353, and trail_44358. The number in each name corresponds to the NORAD catalogue number of the COSMIC-2 satellite that is being trailed. Each MWR satellite is simulated to trail the corresponding COSMIC-2 satellite by 60 seconds.

The trailing MWR satellites are simulated with AMSU-A, ATMS, and the TROPICS Millimeter-wave Sounder (TMS). TMS is a 12 channel microwave radiometer with a 1.5° cross-track sampling interval, 81 soundings per scan, and a maximum scan angle of 60° relative to nadir [13]. The colocations per day found by the RTCD-G method between each trailing MWR satellite and the COSMIC-2 constellation are averaged over 14 days in December 2020. The results are given in Table 5.2.

Table 5.2: Average GNSS-RO/MWR colocations per day estimated by RTCD-G among the COSMIC-2 constellation and the 6 simulated trailing MWR satellites.

	Avg colocations with COSMIC-2 constellation per day		
	AMSU-A	ATMS	TMS
trail_44343	71.2	86.4	125.6
trail_44349	164.6	197.6	281.4
trail_44350	101.5	122.4	179.6
trail_44351	102.9	122.9	175.6
trail_44353	268.6	325.9	513.0
trail_44358	135.6	158.9	223.1
Total	844.4	1014.1	1498.3

The number of found colocations is positively correlated with the maximum scan angle of the MWR instrument used. Simulations with the TMS instrument (maximum scan angle 60°) find the most colocations, simulations with ATMS (maximum scan angle 52.725°) find the second most, and simulations with AMSU-A (maximum scan angle 48.33°) find the least. When the MWR satellites are simulated with AMSU-A instruments, a total of 844.4 colocations are estimated to occur. The colocations are all located in the [-31.8°, 31.8°] latitudinal range. The average number of colocations found in the tropics is 765.7 (90.7%) and the average number of colocations found in the subtropics is 78.7 (9.3%). When the MWR satellites are simulated with ATMS instruments, a total of 1014.1 colocations are estimated to occur among the 6 MWR satellites and 6 COSMIC-2 satellites per day. The colocations are all located in the [-33.4°, 33.4°] latitudinal range. The average number of colocations found in the tropics is 911.6 (89.9%) and the average number of colocations found in the subtropics is 102.5 (10.1%). When the MWR satellites are simulated with TMS instruments, a total of 1498.3 colocations are estimated to occur. The colocations are all located in the [-38.3°, 38.3°] latitudinal range. The average number of colocations found in the tropics is 1315.2 (87.8%), the average number of colocations found in the subtropics is 175.3 (11.7%), and the average number of colocations found outside of the tropics and subtropics is 7.8 (0.5%). The distribution of these colocations in latitude and longitude is shown in Figure 5-2 for an example day (day 345 of 2020).

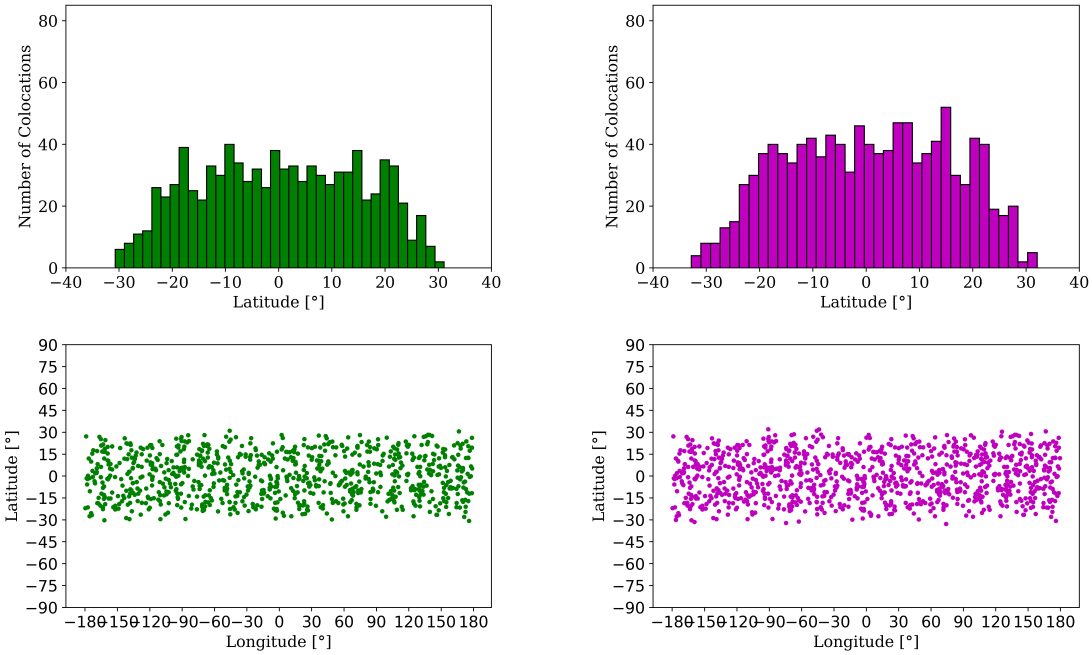

(a) AMSU-A

(b) ATMS

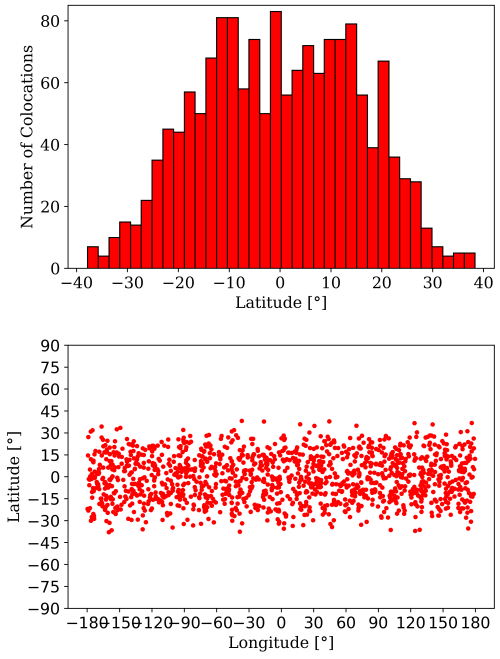

(c) TMS

Figure 5-2: Distribution of all colocations found by the RTCD-G method among the COSMIC-2 constellation and the 6 simulated trailing MWR satellites during day 345 of 2020. Colocations from MWR satellites simulated with AMSU-A, ATMS, and TMS instruments are shown.

Chapter 6

Conclusion

This chapter summarizes the development of the novel method for estimating colocations introduced in this thesis. Results from two applications of the method are explained, and future work is outlined.

6.1 Summary of Findings

6.1.1 Development of RTCD-G and RTCD-SS

The Rotational Transformation Colocation Determination Generalized (RTCD-G) method and the Rotational Transformation Colocation Determination Sun Synchronous (RTCD-SS) methods have been developed as a more efficient alternative to the Brute Force Colocation Determination (BFCD) method typically used in colocation analysis. The rotational methods for colocation determination rotate GNSS-RO soundings into a coordinate system natural to the relevant MWR satellite. Spatial colocation can be assessed by checking if the GNSS-RO sounding occurs within the maximum scan angle of the MWR satellite. Temporal colocation can be assessed by checking if the argument of latitude the MWR satellite would have if it scanned the occultation location is close enough to the actual argument of latitude of the MWR satellite. The rotational methods only require MWR TLE files to predict colocations, rather than the full MWR datasets required by the BFCD method.

6.1.2 Accuracy and Efficiency of RTCD-G

The performance of the RTCD-G method is assessed through comparison to the BFCD method. The RTCD-G method and BFCD method are used to estimate the number of collocations found between COSMIC-2, MetOp-C GRAS, MetOp-C AMSU-A, and NOAA-20 for 12 days in December 2020. The RTCD-G method is found to underestimate the number of colocations, predicting 14.3 less colocations (1.5% less colocated occultations) than the BFCD method per GNSS-RO/MWR combination per day on average. The RTCD-G method finds nearly identical latitudinal and longitudinal distributions of colocations to those found by BFCD. Given the results of the RTCD-G performance assessment, the RTCD-G method has the capability to serve as a conservative estimate for the number of GNSS-RO/MWR colocations found, as well as to identify spatial distribution of colocations. The RTCD-G method proves to be more computationally efficient than the BFCD method. The RTCD-G method predicts daily colocations between GNSS-RO and MWR missions ∼20x faster than the BFCD method on average.

6.1.3 Demonstration of RTCD-G Applications

The RTCD-G method is used for two example applications. The method's computational efficiency is useful to assess colocations among numerous satellites. Colocations occurring among 7 active MWR satellites and 12 active GNSS-RO satellites are analyzed. ∼1300 daily colocations are found among these missions, 60% of which occur in the tropics and subtropics. The 6 satellite GNSS-RO constellation COSMIC-2 is the biggest contributor of colocations, providing over half of the daily colocated occultations. The RTCD-G method's lack of requirement of a full MWR dataset enables easy colocation analysis of theoretical and planned future constellations. The RTCD-G method is applied to analyze colocations resulting from a theoretical constellation designed to produce colocated measurements with COSMIC-2. COSMIC-2 TLE files are adapted to simulate MWR satellites in the same orbits as COSMIC-2 but shifted to trail by one minute in argument of latitude. When simulated with

AMSU-A, ATMS, and TMS instruments, the "trailing" MWR constellation produces ∼850, ∼1015, and ∼1500 daily colocations with COSMIC-2, respectively. Each of these simulated constellations produces more daily colocated COSMIC-2 occultations than the daily amount found among active MWR missions (∼780). The addition of the simulated TMS MWR constellation would more than double the total amount of daily colocations occurring among all active GNSS-RO and MWR satellites considered in this thesis. The two aforementioned applications demonstrate the ability of the RTCD-G method to be an extremely helpful tool in colocation analysis.

6.2 Future Work

6.2.1 Improvements to RTCD-G

The first step to build upon the work presented in this thesis is to improve the accuracy of the RTCD-G method such that its output better aligns with the output of the BFCD method. The RTCD-G method currently only provides a conservative approximation of the true number of colocated occultations.

Improvements to the RTCD-G method will first require further analysis of where the method is failing. Presently, the method assumes that all satellites are in circular Keplerian orbits and that the colocations occur at the time of the colocated radio occultation sounding. Assumptions made by the method must be examined and potentially discarded. Once the failure points of the method are identified, the failure points need to be mitigated while minimizing the loss of any algorithmic efficiency.

6.2.2 Applications of RTCD-G

After improvements are made to the accuracy of the RTCD-G method, the method can be used in various colocation analysis and mission design applications. The RTCD-G method can be used to assess where colocations would occur among theoretical GNSS-RO and MWR satellites in various different orbits.

The work presented in Section 5.2 to design a MWR constellation to maximize

colocations with COSMIC-2 can be built upon. Other MWR constellation architectures should be explored, including a "higher altitude" constellation that involves MWR satellites flying directly above COSMIC-2 satellites.

MWR constellations can be designed to maximize the number of colocated measurements with GNSS-RO satellites in targeted regions of interest. The Marine Boundary Layer in the subtropics, for example, is of particular importance to understanding global weather patterns and requires colocated GNSS-RO/MWR measurements to accurately profile [36]. The RTCD-G method can be used to determine where to locate MWR satellites to enable a high density of colocations in this region.

The RTCD-G method can also be used to investigate various nuances of atmospheric profiling remote sensing missions, such as how many more colocations are produced by GNSS-RO and MWR instruments co-hosted on the same satellite (as opposed to flying on separate satellites), the relative amounts of colocations enabled by different MWR instruments, the potential colocation benefits of flying a constellation of MWR CubeSats rather than a single, large MWR satellite, and how varying theoretical MWR satellite orbital parameters (inclination, eccentricity, etc) affects the amount of colocations with existing and planned GNSS-RO missions.

Appendix A

Code

This appendix gives the Python 3.7 code to implement the colocation determination methods described in this thesis.

A.1 BFCD Algorithm

```
1  import time
2  import os
3  import numpy as np
4  import csv
5  from itertools import zip_longest
6  import matplotlib.pyplot as plt
7
8  def bfcd(mw_sat,ro_sat,time_tolerance,location_tolerance):
9      '''
10     Implements the BFCD method
11
12     Input:
13         MWR satellite object
14         GNSS-RO satellite object
15         Time tolerance for colocation [seconds]
16         Location tolerance for colocation [kilometers]
17
18     Output:
19         Number of colocations found between the MWR and GNSS-RO
20             satellite for a single day
21         List of the latitudes of the colocations found [radians]
22         List of the longitutdes of the colocations found [radians]
23         List of the times of the colocations found [hours since 1/1/70]
24         Total time to run BFCD algorithm [minutes]
25     '''
26
27     if mw_sat.day != ro_sat.day:
28         print('ERROR: mw_sat.day != ro_sat.day')
29
30     start = time.time()
31     print("Starting...")
```

```
32      colocs,counter = 0,0
33      clats, clons, ctimes = [], [], []
34
35      mw_filelist = mw_preload(mw_sat)
36      for file in os.listdir(ro_sat.data):
37          coloc = False
38          counter += 1
39          occult_time, occult_lat, occult_lon, __  = ro_sat.parse_data(file)
40          coloc = bfcd_one_occultation(mw_filelist,occult_time, occult_lat, occult_lon, \
41                                       time_tolerance, location_tolerance)
42
43          if coloc == True:
44              colocs += 1
45              clats.append(occult_lat)
46              clons.append(occult_lon)
47              ctimes.append(occult_time)
48
49      print('number BFCD colocations: ', colocs)
50      end = time.time()
51      time_total = (end - start)/60
52      print('Time: ', time_total)
53
54      ### saving data
55      d = [clats,clons,ctimes]
56      export_data = zip_longest(*d, fillvalue = '')
57      with open(mw_sat.day + '_' + mw_sat.name + '_' + ro_sat.name + '_bfcd.csv', 'w', \
58                encoding="ISO-8859-1", newline='') as myfile:
59            wr = csv.writer(myfile)
60            wr.writerow(("clats", "clons","ctimes"))
61            wr.writerows(export_data)
62      myfile.close()
63      return colocs, clats,clons,ctimes, time_total
64
65  def mw_preload(mw_sat):
66      data_mw = os.listdir(mw_sat.data)
67      file_list = []
68      for l in range(1,len(data_mw)):
69          f = mw_sat.data + str(os.listdir(mw_sat.data)[l])
70          longitudes, latitudes, mid_times = mw_sat.parse_data(f)
71          file_list.append((longitudes, latitudes, mid_times))
72      return file_list
73
74  def bfcd_one_occultation(mw_filelist, ro_time,ro_lat,ro_lon,time_tolerance,location_tolerance):
75      for l in range(0, len(mw_filelist)):
76          longitudes, latitudes, mid_times = mw_filelist[l][0], mw_filelist[l][1], mw_filelist[l][2]
77          for u in range(len(latitudes)):
78              if abs(ro_time - mid_times[u]) < time_tolerance/60/60:
79                  lat_u = latitudes[u]
80                  for c in range(len(lat_u)):
81                      if abs(lat_u[c]-ro_lat) < np.deg2rad(location_tolerance/111):
82                          if np.sqrt((((longitudes[u][c] - ro_lon)**2)*np.cos(ro_lat)**2) + \
83                                     ((lat_u[c] - ro_lat)**2)) < np.deg2rad(location_tolerance/111):
84                              return True
```

A.2 RTCD Algorithm

```
1   import os
```

```
2  import numpy as np
3  import matplotlib.pyplot as plt
4  import time
5
6
7  def RTCD(mw_sat,ro_sat,deltaT,plot_RTCD_rotated):
8      '''
9      Implements the RTCD-G or RTCD-SS method, depending on the type of
10         MWR satelllite object used
11
12     Input:
13         MWR satellite object
14         GNSS-RO satellite object
15         Time tolerance for colocation [seconds]
16         True (create a rotated plot) or false (do not create a rotated plot)
17
18     Output:
19         Number of colocations found between the MWR and GNSS-RO
20             satellite for a single day
21         List of the latitudes of the colocations found [radians]
22         List of the longitutdes of the colocations found [radians]
23         List of the times of the colocations found [hours since 1/1/70]
24         Total time to run RTCD algorithm [minutes]
25     '''
26     start = time.time()
27     print("Starting...")
28
29     if mw_sat.day != ro_sat.day:
30         print('ERROR: mw_sat.day != ro_sat.day')
31
32     p_matrix, times, lats, lons = mw_sat.calc_p_matrix(ro_sat)
33     arg_of_lats, crosstracks, arg_of_lats_timefail, crosstracks_timefail,clats,clons,clats_timefail,\
34     clons_timefail,ctimes = [],[],[],[],[],[],[],[],[]
35     colocs = 0
36
37     for j in range(len(p_matrix[2])):
38
39         #if spatially colocated
40         if abs(np.arcsin(p_matrix[2][j])) < abs(mw_sat.ds):
41
42             u = np.arctan2(p_matrix[1,j],p_matrix[0,j])
43             crosstrack = np.arcsin(p_matrix[2,j])
44             t = times[j]*60*60 #seconds
45
46             n,te,w,M,RAAN,I,e = mw_sat.read_tle(mw_sat.day,t)
47             tau = te - (w+M)/n
48
49             #if temporally colocated
50             if np.cos(u-n*(t-tau)) > np.cos(n*deltaT):
51                 colocs += 1
52                 ctimes.append(times[j])
53
54                 clats.append(np.rad2deg(lats[j]))
55                 clons.append(np.rad2deg(lons[j]))
56                 arg_of_lats.append(np.rad2deg(u))
57                 crosstracks.append(np.rad2deg(crosstrack))
58
59             else:
60                 clats_timefail.append(np.rad2deg(lats[j]))
61                 clons_timefail.append(np.rad2deg(lons[j]))
62                 arg_of_lats_timefail.append(np.rad2deg(u))
```

```
                crosstracks_timefail.append(np.rad2deg(crosstrack))

    if plot_RTCD_rotated == True:
        spatial_and_temporal, = plt.plot(arg_of_lats,crosstracks,'g.',markersize=2)
        spatial_only, = plt.plot(arg_of_lats_timefail,crosstracks_timefail,'r.',markersize=2)
        plt.xlabel('Argument of latitude [degrees]')
        plt.ylabel('Scan distance [degrees]')
        plt.ylim(-90,90)
        plt.yticks(np.arange(-90, 91, step=15))
        plt.xlim(-180,180)
        plt.xticks(np.arange(-180, 181,step=30))
        atms_bounds = plt.axhline(y=np.rad2deg(mw_sat.ds), color='k', linestyle='-')
        plt.axhline(y=np.rad2deg(-mw_sat.ds), color='k', linestyle='-')
        plt.legend([spatial_and_temporal,spatial_only,atms_bounds],['Outside time delta',\
                    'Within time delta','ATMS max scan distance'],markerscale=4.)
        plt.savefig('Day' + str(int(mw_sat.day) - 20000) + '_' + mw_sat.name + '_' + ro_sat.name\
                    +'_RTCD_rotated.png',dpi=500)

    print('number RTCD colocations: ', colocs)
    end = time.time()
    time_total = (end - start)/60
    print('RTCD Time: ', time_total)
    return colocs, clats,clons, ctimes, time_total
```

A.3 Satellite Classes

```
import numpy as np
import os
from netCDF4 import Dataset
import time
import h5py
from astropy.coordinates import TEME, ITRS
from constants import *


class Satellite:
    def __init__(self,name):
        self.name = name

class MWR_SS(Satellite):
    def __init__(self,name,inclination,semi_major_axis,ect,max_scan_angle,time_unit,day):
        '''
        Sun-synchronous MWR satellite object

        Attributes:
            Name of satellite
            Orbital inclination [degrees]
            Semi-major axis [km]
            Equatorial crossing time (ECT) [local time, hours]
            MWR instrument maximum scan angle [degrees]
            Time units of MWR data ['iet' or '1.1.2000']
            Day of year [in TLE form, ie, '20289' for the 289th day of 2020]
        '''
        self.name = name
        self.i = np.deg2rad(inclination)
        self.a = semi_major_axis
        self.Tn = ect
```

```
32          self.xi = np.deg2rad(max_scan_angle)
33          self.time_unit = time_unit
34          self.day = day
35
36          self.ds = np.arcsin((self.a/Earth_Radius)*np.sin(self.xi)) - self.xi
37          self.matrix1 = np.array([[1, 0, 0],
38                                   [0, np.cos(self.i), np.sin(self.i)],
39                                   [0, -np.sin(self.i), np.cos(self.i)]])
40          self.matrix2 = np.array([[np.cos(Earth_Omega*self.Tn),np.sin(Earth_Omega*self.Tn),0 ],
41                                   [-np.sin(Earth_Omega*self.Tn), np.cos(Earth_Omega*self.Tn), 0],
42                                    [0, 0,1]])
43
44          self.data = './' + self.name + '-Data/' + day + '/'
45          self.tle = './TLEs/' + self.name + '.txt'
46
47      def time_conversion(self,times):
48          '''
49          Function to convert MWR sounding times to Unix Epoch Time
50          Input:
51              List of MWR sounding times in IDPS Epoch Time (IET) [Microseconds since
52                  EPOCH of 1 Jan 1958] or 1.1.2000 epoch time [seconds since
53                  1 Jan 2000]
54          Outut:
55              List of MWR sounding times in Unix time converted from seconds to hours
56                  [hours since 1 Jan 1970]
57          '''
58          if self.time_unit == 'idps' or self.time_unit == 'iet':
59              for i in range(len(times)):
60                  if times[i] > 0:
61                      times[i] = times[i]*1e-6 - 378673200.0-18000
62                  else:
63                      times[i] = 0
64          elif self.time_unit == '1.1.2000':
65              for i in range(len(times)):
66                  times[i] = times[i] + 946684800
67          else:
68              print('Error: time units not defined')
69
70          return times/60/60
71
72      def read_tle(self,day,t):
73          '''
74          Function to parse MWR TLE files into the relevent orbital parameters closest
75              to the time of the RO sounding of interest
76          Input:
77              Day of interest [in TLE form, ie, '20289' for the 289th day of 2020]
78              Time of RO sounding [Unix time, seconds]
79
80          Output:
81              MWR orbital parameters from last epoch before occultation time t:
82              n, mean motion [rad/sec]
83              te, time epoch [UTC seconds]
84              w, argument of perigee [radians]
85              M, mean anomaly [radians]
86              RAAN, right ascension of ascending node [radians]
87              i, inclination [radians]
88              e, eccentricity
89          '''
90
91          file = open(self.tle,'r').read()
92          tle_lines = file.strip().splitlines()
```

```
93          lines = []
94          for i in range(len(tle_lines)):
95              if tle_lines[i].split()[0] == '1' and tle_lines[i].split()[3].split('.')[0] == day:
96                  lines.append(i)
97
98          lines.append(lines[-1] + 2)
99          for a in range(len(lines)):
100             current_tle = tle_lines[lines[a]]
101             previous_tle_1 = tle_lines[lines[a]-2] #previous "1" TLE line
102             previous_tle_2 = tle_lines[lines[a]-1] #previous "2" TLE line
103             current_tle_time = 1577836800 + (float(current_tle.split()[3][2:14])-1)*24*60*60
104             if t <= current_tle_time:
105                 RAAN = np.deg2rad(float(previous_tle_2.split()[3]))
106                 e = float('0.'+ previous_tle_2.split()[4])
107                 I = np.deg2rad(float(previous_tle_2.split()[2]))
108                 te = 1577836800 + (float(previous_tle_1.split()[3][2:14])-1)*24*60*60
109                 M = (np.deg2rad(float(previous_tle_2.split()[6])))
110
111                 if self.name[0] != 'c':
112                     n = (float(previous_tle_2.split()[-1][0:11])*2*np.pi/24/60/60)
113                     w = (np.deg2rad(float(previous_tle_2.split()[5])))
114                 else: #code for designing trailing COSMIC-2 constellation
115                     n = (float(previous_tle_2.split()[-2])*2*np.pi/24/60/60)
116                     a = (mu/(n**2))**(1/3)
117                     T = 2*np.pi*np.sqrt(a**3/mu)
118                     frac = 60/T*360
119                     w = (np.deg2rad(float(previous_tle_2.split()[5]))) - np.rad2deg(frac)
120
121                 return n,te,w,M,RAAN,I,e
122
123         print('ERROR: should have found epoch')
124         return n,te,w,M,RAAN,I,e
125
126     def parse_data(self, filename):
127         '''
128         Function to parse full MWR datasets for NOAA-20 and MetOp-C
129         Input:
130             MWR data filename
131         Ouput:
132             List of sounding latitudes [radians]
133             List of sounding longitudes [radians]
134             List of times (one time per cross track scan) [Unix Time seconds]
135         '''
136         if self.name == 'NOAA20':
137             file = h5py.File(filename,'r')
138             longitudes = np.deg2rad(list(file['All_Data/ATMS-SDR-GEO_All/Longitude']))
139             latitudes = np.deg2rad(list(file['All_Data/ATMS-SDR-GEO_All/Latitude']))
140             mid_times = self.time_conversion(np.array(file['All_Data/ATMS-SDR-GEO_All/MidTime']))
141             return longitudes, latitudes, mid_times
142         elif self.name == 'MetOpC-AMSUA':
143             test = Dataset(filename, 'r', format='NETCDF3')
144             latitudes = np.deg2rad(test.variables['lat'][:])
145             longitudes = np.deg2rad(test.variables['lon'][:])
146             record_start_times = self.time_conversion(test.variables['record_start_time'][:])
147             record_stop_times = self.time_conversion(test.variables['record_stop_time'][:])
148             return longitudes, latitudes, record_start_times
149         else:
150             print('ERROR: no satellite with this name')
151             return
152
153     def r_vector(self,lat,lon,tj):
```

```
154             '''
155             Function to compute the RTCD-SS r-vector (position vector in Cartesian  coordinates)
156                 for an RO sounding
157             Input:
158                 Latitude of occultation [radians]
159                 Longitude of occultation [radians]
160                 Time of occultation [Unix time, hours]
161 
162             Output:
163                 r_j (position vector in Cartesian  coordinates)
164             '''
165 
166             r_j = np.array([[np.cos(lon + Earth_Omega*tj)*np.cos(lat)], \
167                             [np.sin(lon + Earth_Omega*tj)*np.cos(lat)],[np.sin(lat)]])
168             return r_j
169 
170         def calc_p_matrix(self,ro_sat):
171             '''
172             Function to perform the RTCD-SS rotational transformation and compute the p matrix
173                 for the given GNSS-RO satellite
174             Input:
175                 GNSS-RO satellite object
176             Outputs:
177                 p_matrix for GNSS-RO satellite object
178                 List of occultation times for GNSS-RO satellite object [Unix time hours]
179                 List of occultation latitudes for GNSS-RO satellite object [Radians]
180                 List of occultation longitudes for GNSS-RO satellite object [Radians]
181             '''
182             r_matrix = np.zeros((3,1))
183             times,lats,lons = [],[],[]
184 
185             for file in os.listdir(ro_sat.data):
186                 occult_time, occult_lat, occult_lon = ro_sat.parse_data(file)
187                 r = self.r_vector(occult_lat, occult_lon, occult_time)
188                 r_matrix = np.append(r_matrix,r,1)
189                 times.append(occult_time)
190                 lats.append(occult_lat)
191                 lons.append(occult_lon)
192             r_matrix = r_matrix[:,1:]
193             p_matrix = self.matrix1 @ self.matrix2 @ r_matrix
194             return p_matrix, times, lats, lons
195 
196 
197     class RO(Satellite):
198         def __init__(self,name,day):
199             '''
200             GNSS-RO satellite object
201 
202             Attributes:
203                 Name of satellite
204                 Day of year [in TLE form, ie, '20289' for the 289th day of 2020]
205             '''
206             self.name = name
207             self.day = day
208             self.data = './' + self.name + '-Data/' + day + '/'
209 
210         def parse_data(self,filename):
211             '''
212             Input:
213                 File containing information about one occultation
214 
```

```
215             Output:
216                 Time of occultation point [Unix time, hours]
217                 Latitude of perigee point at occultation point [Radians]
218                 Longitude of perigee point at occultation point [Radians]
219                 Whether or not the occultation is rising or setting (1 for setting, -1 for rising)
220             '''
221             ncin = Dataset(self.data + filename, 'r', format='NETCDF3')
222             occult_start_time = (ncin.start_time + 315964800)/60/60
223             occult_time = occult_start_time + ncin.occpt_offset/60/60
224             occult_lat = np.deg2rad(ncin.lat)
225             occult_lon = np.deg2rad(ncin.lon)
226             return occult_time, occult_lat, occult_lon,ncin.irs
227
228
229     class MWR_G(MWR_SS):
230         def __init__(self,name,inclination,semi_major_axis,max_scan_angle,day):
231             '''
232             Generalized MWR satellite object
233
234             Attributes:
235                 Name of satellite
236                 Orbital inclination [degrees]
237                 Semi-major axis [km]
238                 MWR instrument maximum scan angle [degrees]
239                 Day of year [in TLE form, ie, '20289' for the 289th day of 2020]
240             '''
241             self.name = name
242             self.i = np.deg2rad(inclination)
243             self.a = semi_major_axis
244             self.xi = np.deg2rad(max_scan_angle)
245             self.day = day
246
247             self.ds = np.arcsin((self.a/Earth_Radius)*np.sin(self.xi)) - self.xi
248             self.matrix1 = np.array([[1, 0, 0],
249                                      [0, np.cos(self.i), np.sin(self.i)],
250                                      [0, -np.sin(self.i), np.cos(self.i)]])
251             self.tle = './TLEs/' + self.name + '.txt'
252
253
254         def r_vector(self,lat,lon,tj):
255             '''
256             Function to compute the RTCD-G r-vector (position vector in Cartesian  coordinates)
257                 for an RO sounding
258             Input:
259                 Latitude of occultation [radians]
260                 Longitude of occultation [radians]
261                 Time of occultation [hours since 1/1/70]
262
263             Output:
264                 Inertial longitude of occultation [radians]
265                 Inertial latitude of occultation [radians]
266             '''
267             #time of occultation
268             p = time.gmtime(tj*60*60)
269             year,month,day,hour,minute, second = p.tm_year,p.tm_mon,p.tm_mday, p.tm_hour, p.tm_min, p.tm_sec
270             tstr = f'{year:4d}-{month:02d}-{day:02d}T{hour:02d}:{minute:02d}:{second:0>10.7f}'
271
272             #r vector in ECEF coordinates
273             r_j = np.array([[np.cos(lon)*np.cos(lat)],[np.sin(lon)*np.cos(lat)],[np.sin(lat)]])
274             occ_ITRS = ITRS( x=r_j[0], y=r_j[1], z=r_j[2], representation_type='cartesian', obstime=tstr )
275
```

```
276         #r vector in TEME coordiantes
277         occ_TEME = np.array( occ_ITRS.transform_to( TEME ).cartesian.xyz )
278         lon_inert = np.arctan2(occ_TEME[1][0],occ_TEME[0][0])
279         lat_inert = np.arctan(occ_TEME[2][0]/np.sqrt(occ_TEME[0][0]**2 + occ_TEME[1][0]**2))
280         return lon_inert, lat_inert
281
282     def calc_p_matrix(self,ro_sat):
283         '''
284         Function to perform the RTCD-G rotational transformation and compute the p matrix
285             for the given GNSS-RO satellite
286         Input:
287             GNSS-RO satellite object
288         Outputs:
289             p_matrix for GNSS-RO satellite object
290             List of occultation times for GNSS-RO satellite object [Unix time hours]
291             List of occultation latitudes for GNSS-RO satellite object [Radians]
292             List of occultation longitudes for GNSS-RO satellite object [Radians]
293         '''
294         p_matrix_big = np.zeros((3,1))
295         times,lats,lons = [],[],[]
296         count = 0
297         for file in os.listdir(ro_sat.data):
298             count += 1
299             occult_time, occult_lat, occult_lon,set_or_rise = ro_sat.parse_data(file)
300             #only consider setting occultations for the MetOp constellation
301             if ro_sat.name == 'MetOpA-GRAS' or ro_sat.name == 'MetOpB-GRAS' or ro_sat.name == 'MetOpC-GRAS':
302                 if set_or_rise == 1:
303
304                     times.append(occult_time)
305                     lats.append(occult_lat)
306                     lons.append(occult_lon)
307                     lon_inert, lat_inert = self.r_vector(occult_lat,occult_lon,occult_time)
308
309                     n,te,w,M,RAAN,I,e = self.read_tle(self.day,occult_time*60*60)
310                     a = (mu/(n**2))**(1/3)/1000
311                     slr = a*(1-e**2)
312                     omega = RAAN + -3/2*n*J2*((Earth_Radius/slr)**2)*np.cos(I)*(occult_time*60*60-te)
313                     matrix2 = np.array([[np.cos(lon_inert - omega)*np.cos(lat_inert)],
314                                         [np.sin(lon_inert - omega)*np.cos(lat_inert)],
315                                         [np.sin(lat_inert)]])
316                     p_matrix = self.matrix1 @ matrix2
317                     p_matrix_big = np.append(p_matrix_big,p_matrix,1)
318             else:
319                 times.append(occult_time)
320                 lats.append(occult_lat)
321                 lons.append(occult_lon)
322                 lon_inert, lat_inert = self.r_vector(occult_lat,occult_lon,occult_time)
323
324                 n,te,w,M,RAAN,I,e = self.read_tle(self.day,occult_time*60*60)
325                 a = (mu/(n**2))**(1/3)/1000
326                 slr = a*(1-e**2)
327                 omega = RAAN + -3/2*n*J2*((Earth_Radius/slr)**2)*np.cos(I)*(occult_time*60*60-te)
328                 matrix2 = np.array([[np.cos(lon_inert - omega)*np.cos(lat_inert)],
329                                     [np.sin(lon_inert - omega)*np.cos(lat_inert)],
330                                     [np.sin(lat_inert)]])
331                 p_matrix = self.matrix1 @ matrix2
332                 p_matrix_big = np.append(p_matrix_big,p_matrix,1)
333         p_matrix_big = p_matrix_big[:,1:]
334
335         return p_matrix_big, times, lats, lons
```

A.4 Example Satellite Object Definitions

```
day = '20337'

#ro sats
cosmic2 = RO('COSMIC2',day)
MetOpA_GRAS = RO('MetOpA-GRAS',day)
MetOpB_GRAS = RO('MetOpB-GRAS',day)
MetOpC_GRAS = RO('MetOpC-GRAS',day)
PAZ = RO('PAZ',day)
TSX = RO('TSX',day)
TDX = RO('TDX',day)

#mwr sats (RTCD-G)
noaa_18 = MWR_G('NOAA18', 99.0, 7228.75,48.33, day)
noaa_19 = MWR_G('NOAA19', 99.2,7229,48.33, day)
noaa_20 = MWR_G('NOAA20',98.74,7205,52.725, day)
SNPP = MWR_G('SNPP',98.7,7205,52.725, day)
MetOpA_AMSUA = MWR_G('MetOpA-AMSUA',98.7, 7198.5, 48.33,day )#8.7666
MetOpB_AMSUA = MWR_G('MetOpB-AMSUA',98.7, 7198.5, 48.33,day )
MetOpC_AMSUA = MWR_G('MetOpC-AMSUA',98.7, 7198.5, 48.33,day )

#mwr sats (RTCD-SS)
noaa_20 = MWR_SS('NOAA20',98.74,7205,13.416,52.725,'idps',day)
MetOpC_AMSUA = MWR_SS('MetOpC-AMSUA',98.7, 7198, 12+9.5, 48.33, '1.1.2000',day )
```

A.5 Constants

```
J2 = 1.08262668*10**-3 #J2 perturbation [unitless]
Earth_Radius = 6371 #Radius of Earth [km]
Earth_Omega = (2*np.pi)/(24) #Solar fixed spin rate of Earth [radians per hour]
mu = 3.986004418*10**14 #Earth standard gravitational parameter [m3 per s2]
```

Bibliography

[1] Noaa center for satellite applications and research (star) integrated calibration/-validation system (icvs) long-term monitoring: Metop-c amsu-a. Available at =https://www.star.nesdis.noaa.gov/icvs/status$_{M}etOPC_{A}MSUA.php$.

[2] Orbital coordinate systems, part i. Available at =https://celestrak.com/columns/v02n01/.

[3] rohp-paz introduction. Available at =https://paz.ice.csic.es/introduction.php?idi=EN.

[4] World meteorological organization oscar (observing systems capability analysis and review tool). Available at =https://www.wmo-sat.info/oscar/instruments.

[5] Radio occultation. Available at =https://scied.ucar.edu/radio-occultation-for-teaching-box, 2018.

[6] Report to congress: Radio occultation data gap mitigation plan, 2020. Report to Congress.

[7] Cdaac gnss radio occultation datasets. Available at =https://www.cosmic.ucar.edu/what-we-do/data-processing-center/data/, 2021.

[8] Noaa comprehensive large array-data stewardship system (class). Available at = https://www.avl.class.noaa.gov/saa/products/search?datatype$_{f}amily$ = $ATMS_{S}DR$, 2021.

[9] R. Anthes. Exploring earth's atmosphere with radio occultation: Contributions to weather, climate and space weather. *Atmospheric Measurement Techniques Discussions*, 4, 06 2011.

[10] D. S. Arndt, M. O. Baringer, and M. R. Johnson. State of the climate in 2009. *Bulletin of the American Meteorological Society*, 91(7):s1 – s222, 01 Jul. 2010.

[11] Weihua Bai, Nan Deng, Yueqiang Sun, Qifei Du, Junming Xia, Xianyi Wang, Xiangguang Meng, Danyang Zhao, Congliang Liu, Guangyuan Tan, Ziyan Liu, and Xiaoxu Liu. Applications of gnss-ro to numerical weather prediction and tropical cyclone forecast. *Atmosphere*, 11(11), 2020.

[12] Peter Bauer, Alan Thorpe, and Gilbert Brunet. The quiet revolution of numerical weather prediction. *Nature*, 525:47–55, 09 2015.

[13] William J. Blackwell. An overview of the nasa tropics earth venture mission. In *2017 IEEE International Geoscience and Remote Sensing Symposium (IGARSS)*, pages 5934–5937, 2017.

[14] C. Cardinali and S. Healy. Impact of gps radio occultation measurements in the ecmwf system using adjoint-based diagnostics. *Quarterly Journal of the Royal Meteorological Society*, 140:2315–2320, 2014.

[15] Shu-Ya Chen, Chian-Yi Liu, Ching-Yuang Huang, Shen-Cha Hsu, Hsiu-Wen Li, Po-Hsiung Lin, Jia-Ping Cheng, and Cheng-Yung Huang. An analysis study of formosat-7/cosmic-2 radio occultation data in the troposphere. *Remote Sensing*, 13(4), 2021.

[16] William Emery and Adriano Camps. Chapter 8 - atmosphere applications. In William Emery and Adriano Camps, editors, *Introduction to Satellite Remote Sensing*, pages 597–636. Elsevier, 2017.

[17] S. English, Richard Renshaw, P. Dibben, A. Smith, P. Rayer, C. Poulsen, F. Saunders, and J. Eyre. A comparison of the impact of tovs and atovs satellite sounding data on the accuracy of numerical weather forecasts. *Quarterly Journal of the Royal Meteorological Society*, 126:2911 – 2931, 10 2000.

[18] U. Foelsche, B. Scherllin-Pirscher, F. Ladstädter, A. K. Steiner, and G. Kirchengast. Refractivity and temperature climate records from multiple radio occultation satellites consistent within 0.05 *Atmospheric Measurement Techniques*, 4(9):2007–2018, 2011.

[19] G. Goodrum, K.B. Kidwell, W. Winston, R. Aleman, and National Climatic Data Center (U.S.). Satellite Services Branch. *NOAA KLM User's Guide*. U.S. Department of Commerce, National Oceanic and Atmospheric Administration, National Environmental Satellite, Data, and Information Service, National Climatic Data Center, Climate Services Division, Satellite Services Branch, 1999.

[20] George Vadimovich Gruza and I G Sitnikov. *Principal Weather Systems in Subtropical and Tropical Zones*, volume 1. Eolss Publishers, 2009.

[21] Xueyan Hou, Yang Han, Xiuqing Hu, and Fuzhong Weng. Verification of fengyun-3d mwts and mwhs calibration accuracy using gps radio occultation data. *Journal of Meteorological Research*, 33, 05 2019.

[22] Robbie Iacovazzi, Lin Lin, Ninghai Sun, and Quanhua Liu. Noaa operational microwave sounding radiometer data quality monitoring and anomaly assessment using cosmic gnss radio-occultation soundings. *Remote Sensing*, 12(5), 2020.

[23] Oscar Isoz, S. Buehler, and P. Eriksson. Intercalibration of microwave temperature sounders using radio occultation measurements. *Journal of Geophysical Research*, 120:3758–3773, 2015.

[24] N. Jakowski. Radio occultation techniques for probing the ionosphere. *URSI Radio Science Bulletin*, 2005(314):4–15, 2005.

[25] M. Janssen. *Atmospheric Remote Sensing by Microwave Radiometry*, volume 36. 01 1993.

[26] Thomas Jennings. *Joint Polar Satellite System (JPSS) Common Data Format Control Book – External*, volume I. NASA Goddard Space Flight Center, 2011.

[27] Edward Kim, Cheng-Hsuan Lyu, Kent Anderson, R. Leslie, and William Blackwell. S-npp atms instrument prelaunch and on-orbit performance evaluation. *Journal of Geophysical Research: Atmospheres*, 119, 05 2014.

[28] T. J. Kleespies. Relative information content of the advanced technology microwave sounder and the combination of the advanced microwave sounding unit and the microwave humidity sounder. *IEEE Transactions on Geoscience and Remote Sensing*, 45(7):2224–2227, 2007.

[29] F. Ladstädter, H. Gleisner, K. Kinch, K. B. Lauritsen, U. Foelsche, C. Marquardt, J. Ackermann, and A. von Engeln. Collocating GRAS with AMSU onboard of Metop: An assessment for instrument and climate monitoring. In *EGU General Assembly Conference Abstracts*, EGU General Assembly Conference Abstracts, page 10298, April 2012.

[30] Qifeng Lu and W. Bell. Characterising channel center frequencies in amsu-a and msu microwave sounding instruments. (700):29, 05 2013.

[31] W. Melbourne, E. S. Davis, C. Duncan, G. Hajj, K. Hardy, E. R. Kursinski, T. Meehan, L. Young, and T. Yunck. The application of spaceborne gps to atmospheric limb sounding and global change monitoring. 1994.

[32] S. Sokolovskiy. Algorithms for inverting radio occultation signals in the neutral atmosphere. Available at =https://cdaac-www.cosmic.ucar.edu/cdaac/doc/documents/roam05.doc.

[33] Sergey Sokolovskiy. Effect of superrefraction on inversions of radio occultation signals in the lower troposphere. *Radio Science - RADIO SCI*, 38:24–1, 06 2003.

[34] JPSS ATMS SDR Science Team. Joint polar satellite system advanced technology microwave sounder (atms) sdr radiometric calibration algorithm theoretical basis document (atbd). *Center for Satellite Applications and Research*, 2013.

[35] A. von Engeln, Y. Andres, C. Marquardt, and F. Sancho. Gras radio occultation on-board of metop. *Advances in Space Research*, 47(2):336–347, 2011. Scientific applications of Galileo and other Global Navigation Satellite Systems - I.

[36] Kuo-Nung Wang, Manuel Juarez, Ono Ao, and F. Xie. Correcting negatively-biased refractivity below ducts in gnss radio occultation: An optimal estimation approach towards improving planetary boundary layer (pbl) characterization. *Atmospheric Measurement Techniques Discussions*, pages 1–32, 04 2017.

[37] Fuzhong Weng. *Passive Microwave Remote Sensing of the Earth.* John Wiley & Sons Ltd, Weinheim, Germany, 2017.

[38] Fuzhong Weng and Hu Yang. Validation of atms calibration accuracy using suomi npp pitch maneuver observations. *Remote Sensing*, 8(4), 2016.

[39] Ed Westwater, Susanne Crewell, Christian Matzler, and D. Cimini. Principles of surface-based microwave and millimeter wave radiometric remote sensing of the troposphere. *Quaderni della Societ Italiana di Elettromagnetismo*, 1, 01 2005.

[40] F. Xie, Dong wu, Ono Ao, Rob Kursinski, Anthony Mannucci, and S. Syndergaard. Super-refraction effects on gps radio occultation refractivity in marine boundary layers. *Geophysical Research Letters - GEOPHYS RES LETT*, 37, 06 2010.

[41] Feiqin Xie, Stig Syndergaard, E. Robert Kursinski, and Benjamin M. Herman. An approach for retrieving marine boundary layer refractivity from gps occultation data in the presence of superrefraction. *Journal of Atmospheric and Oceanic Technology*, 23(12):1629 – 1644, 01 Dec. 2006.

[42] Banghua Yan, Junye Chen, Cheng-Zhi Zou, Khalil Ahmad, Haifeng Qian, Kevin Garrett, Tong Zhu, Dejiang Han, and Joseph Green. Calibration and validation of antenna and brightness temperatures from metop-c advanced microwave sounding unit-a (amsu-a). *Remote Sensing*, 12(18), 2020.

[43] Cheng-zhi Zou, Mitchell Goldberg, and Xianjun Hao. New generation of u.s. satellite microwave sounder achieves high radiometric stability performance for reliable climate change detection. *Science Advances*, 4, 10 2018.

[44] X. Zou, Zhengkun Qin, and F. Weng. Impacts from assimilation of one data stream of amsu-a and mhs radiances on quantitative precipitation forecasts: Impact of satellite data assimilation on qpf. *Quarterly Journal of the Royal Meteorological Society*, 143, 11 2016.